Gondwana Research 84 (2020) 211–228

Contents lists available at ScienceDirect

Gondwana Research

journal homepage: www.elsevier.com/locate/gr

The oldest record of Ediacaran macrofossils in Gondwana (~563 Ma, Itajaí Basin, Brazil)

Bruno Becker-Kerber [a,b,*], Paulo Sergio Gomes Paim [c], Farid Chemale Junior [c], Tiago Jonatan Girelli [c], Ana Lucia Zucatti da Rosa [d], Abderrazak El Albani [b], Gabriel Ladeira Osés [a], Gustavo M.E.M. Prado [e], Milene Figueiredo [f], Luiz Sérgio Amarante Simões [g], Mírian Liza Alves Forancelli Pacheco [h,i]

[a] Programa de Pós-Graduação em Ecologia e Recursos Naturais, Universidade Federal de São Carlos, São Carlos, SP, Washington Luiz, 325km, 13565-905, Brazil
[b] Unité Mixte de Recherche (UMR), Centre National de la Recherche Scientifique (CNRS), IC2MP 7285, University of Poitiers, 86073 Poitiers, France
[c] Programa de Pós-Graduação em Geologia, Universidade do Vale do Rio dos Sinos, 93.022-750 São Leopoldo, RS, Brazil
[d] Petrobras, Santos, SP, Brazil
[e] Instituto de Geociências, Universidade de São Paulo, Rua do Lago, 562, Cidade Universitária, São Paulo, SP 05508-080, Brazil
[f] Petrobras Research Centre – CENPES, Brazil
[g] Instituto de Geociências e Ciências Exatas (IGCE), Universidade Estadual Paulista (UNESP), Rio Claro, SP, Brazil
[h] Departamento de Biologia, Universidade Federal de São Carlos – campus Sorocaba, Rod. João Leme dos Santos km 110, CEP 18052-780 Sorocaba, Brazil
[i] Instituto de Física, Universidade de São Paulo, Rua do Matão, Travessa R 187, CEP 05508-090 São Paulo, Brazil

ARTICLE INFO

Article history:
Received 11 October 2019
Received in revised form 11 March 2020
Accepted 12 March 2020
Available online 1 May 2020

Editor: M. Santosh

ABSTRACT

The Avalon biota (Ediacaran Period, 570–559 Ma) marks the first appearance of macroscopic and complex benthic communities in the fossil record. This assemblage is known from a few localities worldwide, mainly in Canada and England. Here, we report for the first time the presence of Ediacaran macrofossils in deposits of similar age from Gondwana (Itajaí Basin, southern Brazil). Our new radiometric date (~563 Ma) indicates that the Itajaí Basin can be chronocorrelated with the classic Avalonian deposits and thus represents one of the oldest records of the Ediacaran biota in Gondwana. We describe the presence of the Ediacaran genus *Palaeopascichnus*, as well as discs (*Aspidella* and *Nimbia*), and other problematic forms. Contrary to the deep-marine macroorganisms of the Avalon Assemblage, the Itajaí fossils are associated with abundant and exceptionally preserved three-dimensional microbial mats and microbially induced sedimentary structures (MISS) in relatively shallow settings (upper slope and distal delta front deposits). In this sense, the Itajaí biota could represent early adaptations of benthic macrobiota to the shallower and more photic environments that characterize the later White Sea Assemblage.

1. Introduction

The first fossil evidence of macroscopic complex life forms is preserved in rocks associated with deep aphotic environments in the middle-late Ediacaran Period (Liu et al., 2015 and references therein). The appearance of this Ediacaran biota marked the development of macroscopic benthic ecosystems characterized by an "explosion" of morphospace (i.e., Avalon biota) (Shen et al., 2008), including possible stem-group metazoans (Liu et al., 2015). Subsequent biotas include the White Sea and Nama Assemblages, which have distinct biotic compositions and further evolutionary innovations (e.g., mobility and skeletonized animals, respectively) and were associated with shallow waters and photic zones (Grazhdankin, 2004; Boag et al., 2016).

Despite this knowledge, the mechanisms and biases behind the transitions among these biotas still need to be better understood. It is likely that both biological and environmental changes played a synergic role in ecosystem structuration during the Ediacaran. Specifically, the Avalon and White Sea biotas differ dramatically in the sense that the latter contains the first macroscopically complex organisms that were adapted to shallow waters and were associated with abundant textured organic surfaces (Droser et al., 2017).

Studies on the Avalonian biotas have mostly been restricted to the widely investigated rocks in Canada and England (Ford, 1958; Misra, 1969; Boynton and Ford, 1995; Narbonne and Gehling, 2003; Hofmann et al., 2008; Narbonne et al., 2014; Liu et al., 2015). Therefore, exploring the paleontological potential of other coeval deposits is essential to developing a more complete picture of the early evolution of macroscopic life.

* Corresponding author at: Programa de Pós-Graduação em Ecologia e Recursos Naturais, Universidade Federal de São Carlos, São Carlos, SP, Washington Luiz, 325km, 13565-905, Brazil.
E-mail addresses: beckerkerber@gmail.com (B. Becker-Kerber), ppaim@unisinos.br (P.S.G. Paim), FARIDCJ@unisinos.br (F. Chemale Junior), abder.albani@univ-poitiers.fr (A.E. Albani), lsimoes@rc.unesp.br (L.S.A. Simões), forancelli.ufscar@gmail.com (M.L.A.F. Pacheco).

https://doi.org/10.1016/j.gr.2020.03.007
1342-937X/

To date, Ediacaran units in South America bearing putative soft-bodied taxa have been reported only in deposits near the Ediacaran-Cambrian transition (Gaucher, 2018) and require further investigations regarding their proposed body fossil content (Inglez et al., 2019).

One geologic unit with great potential for studies on Ediacaran biota is the Itajaí Basin (IB). This geologic unit has long been controversial in terms of its paleontological record, mostly due to scarce studies. Previous and mostly unpublished works have suggested the presence of Cambrian (*Chancelloria* and *Choia*) and Ediacaran taxa (*Aspidella*), as well as putative ichnofossils such as *Diplocraterion*, *Helmintoidichnites*, and *Oldhamia* (Da Rosa et al., 1997; Leipnitz et al., 1997; Paim et al., 1997). These claims have led to some uncertainty about the age of the basin since radiometric dating suggested an upper Neoproterozoic age (Guadagnin et al., 2010; Basei et al., 2011 and references therein).

This study reports new fossil findings and geochronological data for the Itajaí Group. Here, we show the presence of macroorganisms, as well as putative animals, and abundant microbially induced sedimentary structures (MISS) associated with settings that are shallower than those of other Avalonian deposits. In this sense, the Itajaí biota can be considered a key locality for understanding the colonization of shallower (and possibly photic) environments by complex Ediacaran organisms.

2. Geological context

During the late to postorogenic stages of the Pan-African-Brasiliano Orogeny (~600–540 Ma), several sedimentary basins formed as a result of the collision of the Rio de la Plata, Congo and Kalahari cratons (Gresse et al., 1996). They include the Itajaí (Guadagnin et al., 2010; Basei et al., 2011), Camaquã (Paim et al., 2000; Netto, 2012), Arroyo del Soldado (Gaucher, 2000; Blanco et al., 2009) and Nama (Saylor et al., 1995; Grotzinger et al., 1995) basins (Supplementary Fig. 1), among others, and the IB is the focus of this work.

The E-NE-elongated IB is interpreted as a foreland basin (Rostirolla, 1991; Rostirolla et al., 1992; Gresse et al., 1996; Guadagnin et al., 2010) related to the Dom Feliciano Belt (DFB) in Santa Catarina State (Supplementary Fig. 1). The DFB comprises, from east to west, the Florianópolis Magmatic Arc, the metavolcano-sedimentary Brusque Complex and the foreland IB. To the northwest, the IB covers the Santa

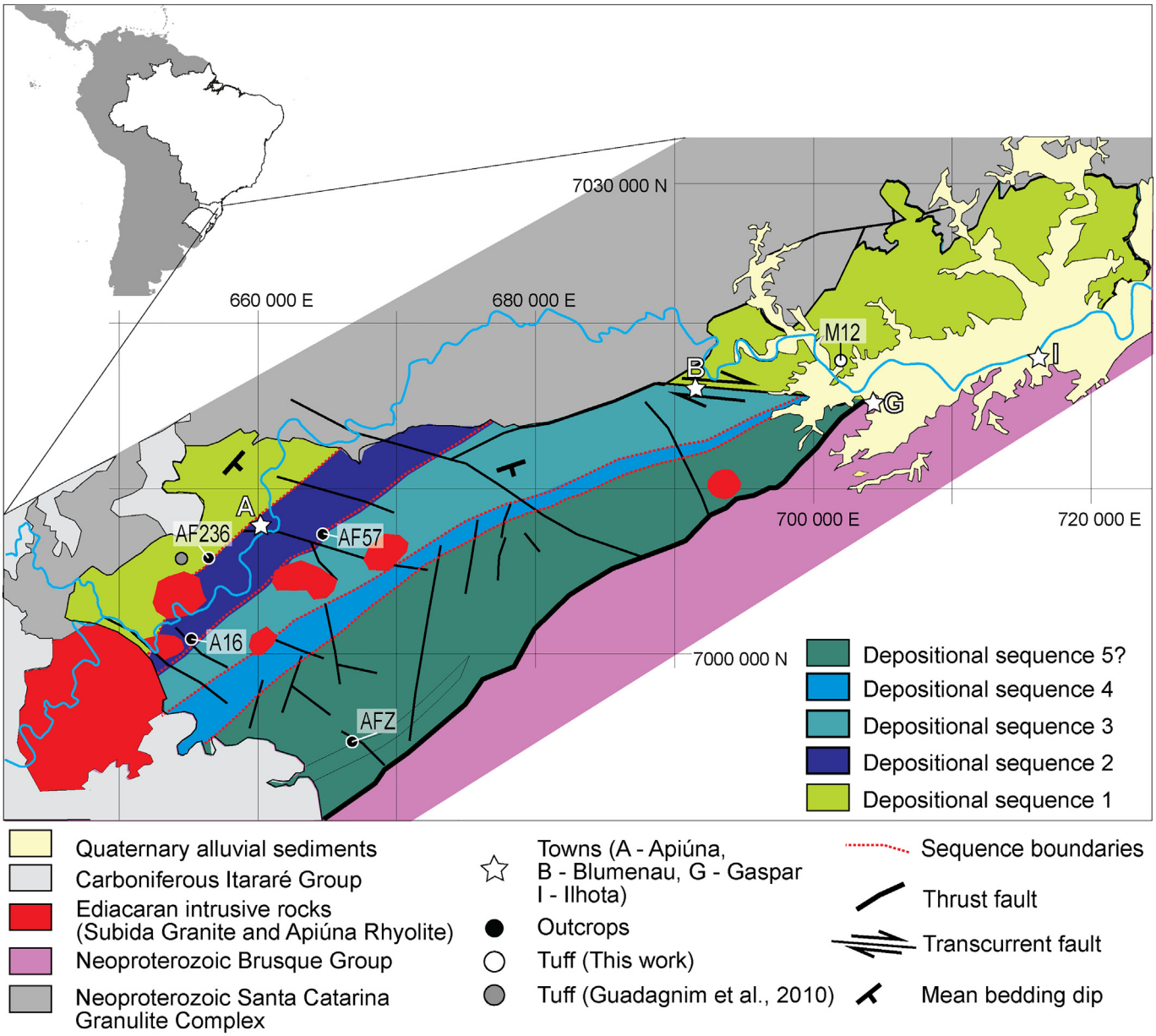

Fig. 1. Simplified geological map of the Itajaí Basin showing the main depositional sequences (DS) (modified after Fonseca, 2004 and Teixeira et al., 2004) and main fossiliferous outcrops.

Catarina Granulite Complex, a tectonically stable area related to the Luis Alves Microplate (Guadagnin et al., 2010; Basei et al., 2011) (Fig. 1). The IB contains a thick siliciclastic succession, with minor volcaniclastic strata, that was deposited between 572 and 549 Ma (Guadagnin et al., 2010). This succession includes alluvial, deltaic and shallow- to deep-marine strata organized into five depositional sequences (adapted from Fonseca, 2004 and Teixeira et al., 2004 (Fig. 1)).

Depositional sequence 1 (DS1) encompasses a transgressive systems tract characterized by alluvial conglomerates and sandstones followed by deltaic to shallow-marine sandstones to siltstones and rarer shales (Figs. 1, 2). The alluvial and delta plain facies include trough cross-bedded, fining-upward lenses of clast-supported conglomerates and sandstones related to braided streams. The trough cross-bedded sets are bounded by low-angle, down-current dipping surfaces related to the frontal accretion of fluvial braid bars. The shallow-marine deposits are composed of fine- to medium-grained, well-sorted sandstone lenses displaying swaley and hummocky cross-bedding and rarer wave ripples associated with wave-dominated coastal areas. Finally, the delta front and prodelta facies encompass coarsening- and thickening-upward packages of thin-bedded siltstones and rarer shales and fine- to very fine-grained, massive or climbing ripple sandstones (distal delta front to prodelta) overlain by massive, meter-scale sandstone lenses (proximal delta front).

A relatively deep-marine succession (DS2), mostly composed of high-density, channelized to unconfined turbidites (Apiúna Turbidite Complex) and fine-grained, slope to basinal facies, unconformably overlies the previous units and represents a succeeding lowstand systems tract. Turbidite channels comprise meter- to a few tens of meters-wide and several meters-thick lenses composed of matrix-supported conglomerates and/or very coarse- to coarse-grained, massive sandstones. The turbidite channel fill usually exhibits fining-upward trends and abundant rip-up clasts near their erosional bases and are surrounded by thin-bedded, fine-grained slope deposits. Slumped beds are rare. Unconfined, more distal turbidite deposits are tabular and composed of decimeter-scale beds of fine- to very fine-grained, massive to planar-bedded sandstones (turbidite lobe) and centimeter-scale couplets of fine- to very fine-grained sandstone and siltstone (lobe fringe). The transition between channelized and nonchannelized turbidite facies is gradual.

An erosional, subaerial unconformity highlighted by fluvial facies resting immediately above the slope strata of the previous depositional sequence delineates the base of the subsequent succession

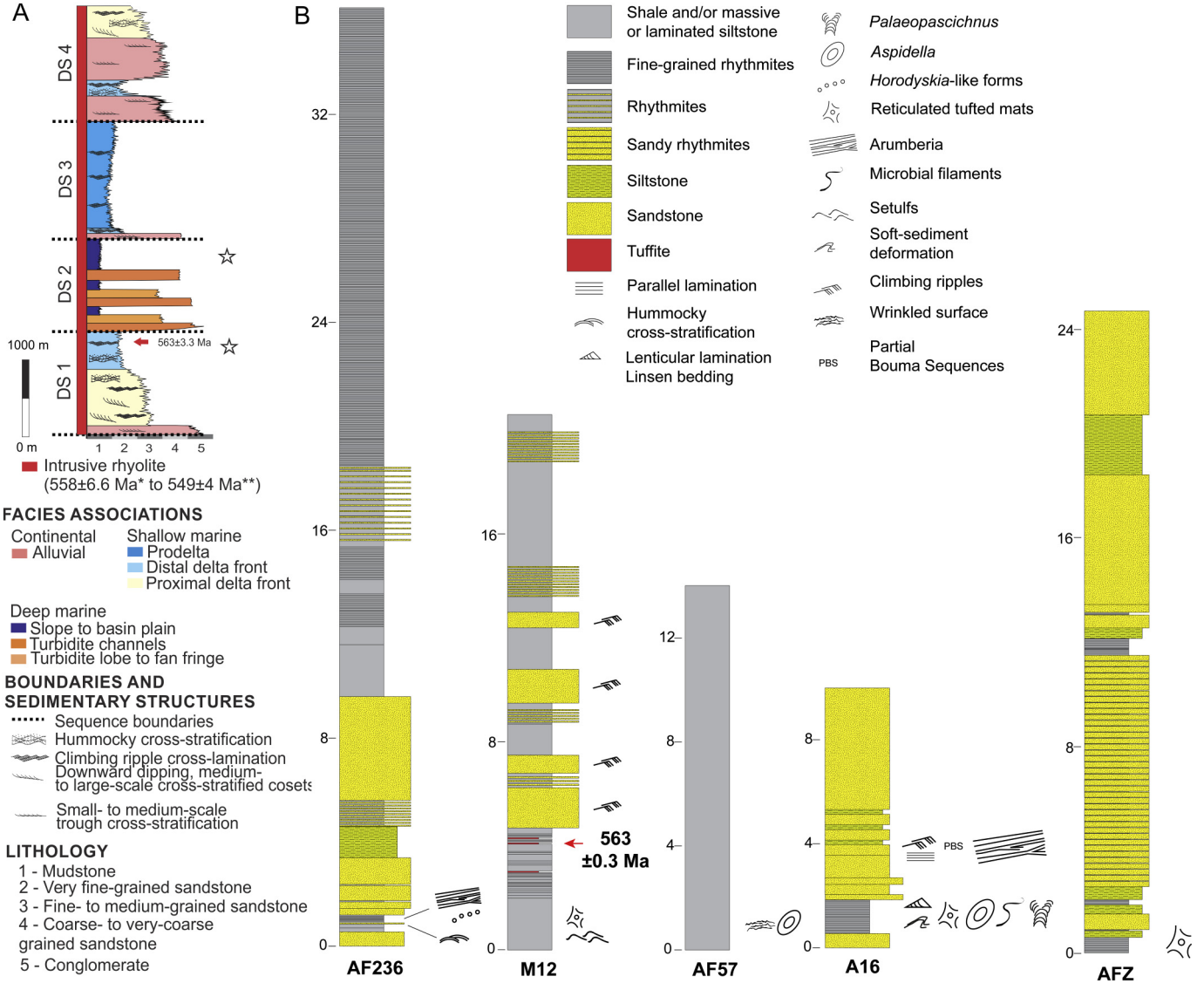

Fig. 2. A) Simplified composite column displaying depositional sequences DS1 to DS4, facies associations, related grain size trends, main sedimentary structures, estimated positions of fossil horizons (stars), and dated tuff layer (red arrow) (based on Fonseca, 2004); B) Profiles of the studied sections. *After Basei et al. (2011). **After Guadagnin et al. (2010).

(DS3), which is mostly composed of deltaic to shallow-marine deposits that display features similar to those of DS1. The subsequent depositional sequence (DS4) repeats the previous sequence, including the presence of fluvial strata above a subaerial unconformity scoured into marine deposits of DS3. However, DS4 includes a larger proportion of fluvial and proximal, wave-influenced delta front sandstones than DS3. Above the fourth depositional sequence, a thick, strongly deformed, and partially inverted package (DS5) containing turbidite, delta front to prodelta, and alluvial strata occurs. However, its actual stratigraphic position is still uncertain. Whereas Rostirolla (1991), Fonseca (2004), and Guadagnin et al. (2010) describe it as the youngest sequence of the IB, Basei et al. (2011) suggest that this unit has been overthrusted onto the underlying units. The turbiditic, delta front to prodelta, and alluvial facies are similar to those described in more detail in DS1 and DS2.

The studied fossils and MISS were found in shallow- to relatively deep-marine strata (Figs. 1–3, and Supplementary Fig. 2), including the fine-grained, distal delta front facies of DS1 (e.g., outcrops AF236 and M12) and the upper slope facies (fine-grained, thin-bedded turbidites) close to the subaerial unconformity that delineates the DS2 upper boundary (e.g., outcrop A16). The fossils occur in millimetric rhythmites of clay, silt and fine-grained sand. Body fossils and/or microbial mats were not found in the deeper facies of DS2. No true palynomorphs were recovered from palynological macerations, but artifacts of particulate organic material were observed during the investigation (Supplementary Text 1).

3. Material and methods

3.1. Samples and localities

We prospected approximately 234 outcrops (Supplementary Fig. 2, Supplementary Table) throughout the basin during field work, but the majority of samples were collected in the more prolific localities AF236, M12, A16, AF57, and AFZ (Figs. 1, 2). The samples were collected in situ, except for sample CAP/1A–558, which was found in the float. All hand samples, including body fossils and MISS ($n = 295$), analyzed here have been deposited in the "Coleção Arqueológica e Paleontológica" (CAP-549–582 and CAP-877–1019) at the Universidade Federal de São Carlos (Sorocaba, Brazil).

3.2. Macroscopic and petrographic investigation

Polished sections parallel and transverse to the bedding plane were made to examine the biological and sedimentary features under a STEREO Discovery V20 stereomicroscope coupled with an Axiocam camera at the Laboratório de Ecologia at the Universidade Federal de Mato Grosso do Sul. Thin sections were prepared at the Programa de Pós-Graduação em Geologia da Universidade do Vale do Rio dos Sinos (UNISINOS – São Leopoldo) and at the Setor de Laminação of the UNESP (Rio Claro). The thin sections were analyzed under a Leica microscope at the Instituto de Geociências of Universidade de São Paulo (IGc-USP).

3.3. Scanning electron microscopy and μX-ray fluorescence

Scanning electron microscopy (SEM) analyses were performed using Quanta 650FEG and FEI Inspect F50 microscopes at the Brazilian National Laboratory of Nanotechnology (LNNano/CNPEM), both in high-vacuum mode and with a current tension of 15 kV. Synchrotron radiation μX-ray fluorescence (SR-μXRF) mapping was performed at the Brazilian Synchrotron Light Laboratory (LNLS), and measurements were made using polychromatic excitation in microbeam mode and filtering with Fe foils. The FlyScan mode was used with 500 ms of count time per point. The data were later treated with PyMCA software.

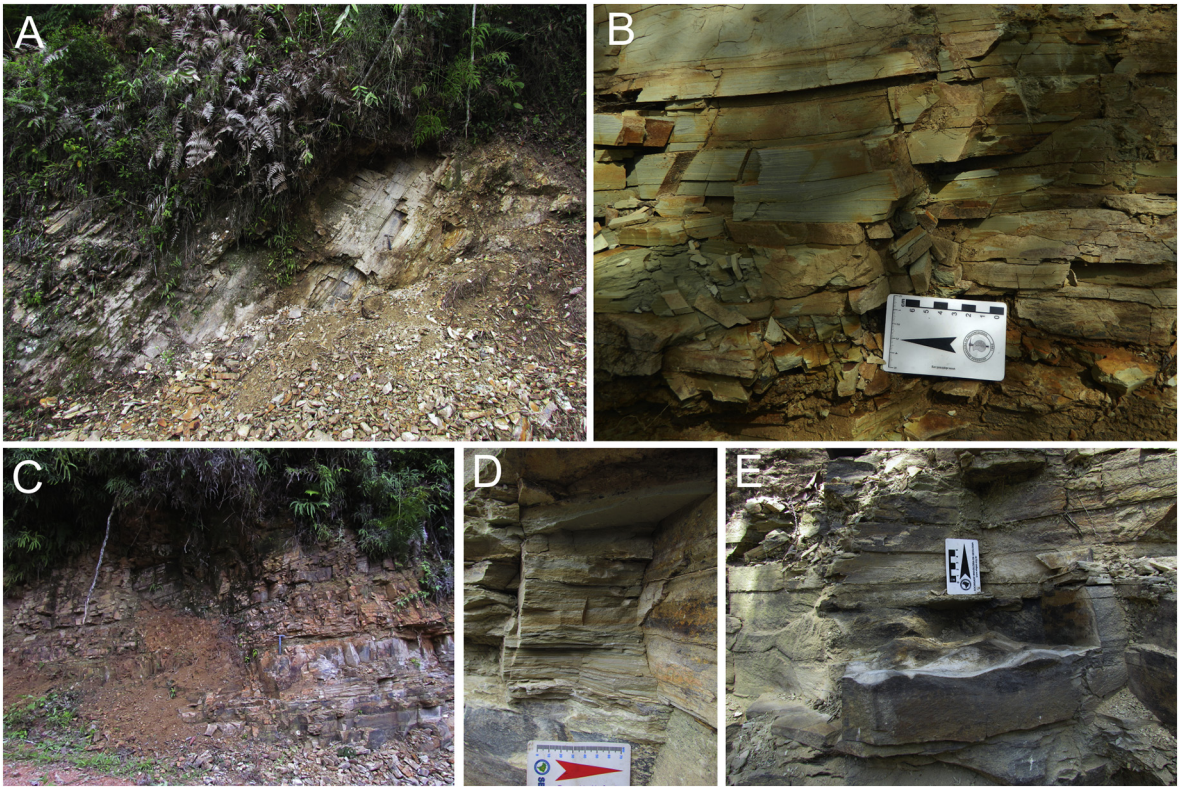

Fig. 3. Photographs of the main fossiliferous localities. A–B) Outcrop A16 (depositional sequences 2–3); B) Detail of the fossiliferous fine-grained rhythmites present in A16; C–E) Outcrop AF236 (depositional sequence 1); D) Detail of the fossiliferous horizon characterized by fine-sandstone/mudstone intercalations; E) Wave-rippled sandstone at the same locality.

3.4. U-Pb geochronology

Zircon grains were separated from a felsic tuff layer (sample T2A1M12; Figs. 1, 2) after crushing and milling using a jaw crusher and ring mill apparatus. Heavy and light minerals were separated using heavy liquids and a Frantz® magnetic separator after concentration of minerals by manual panning. Handpicked zircon crystals were mounted in an epoxy disc, ground and polished. Reflected light photomicrographs of samples were obtained, and images were produced using a scanning electron microscope for backscattered electron (BSE) and cathodoluminescence (CL) imaging. In situ laser ablation inductively coupled plasma mass spectrometry (LA-ICP-MS) U-Pb zircon dating was carried out at the Isotope Geology Laboratory of Universidade Federal de Ouro Preto (Brazil) using a Photon-machines ArF excimer laser 193 coupled to a high-resolution sector field inductively coupled plasma mass spectrometer (HR-SF-ICP-MS, Element 2). A laser spot size of 30 μm was used, and data were acquired in peak jumping mode during a 20-s background measurement followed by a 20-s sample ablation. To evaluate the accuracy and precision of the laser ablation results, the zircon reference materials BB-1 (Santos et al., 2017), Plešovice (Sláma et al., 2008) and GJ-1 (Jackson et al., 2004) were also analyzed. The obtained ages agreed within the experimental errors: 563.8 ± 3.2 Ma ($n = 14$) for BB-1, 601.3 ± 2.8 Ma ($n = 12$) for GJ-1 and 338.4 ± 2.2 Ma (n = 12) for Plešovice. The raw data were corrected for background signal, and laser-induced elemental fractional and instrumental mass discriminations were corrected by the reference zircon BB-1. The common Pb correction was based on the measured ^{204}Pb composition (of the sample) following the model of Stacey and Kramers (1975). The decay constant values used were from Jaffey et al. (1971). The data were corrected and reduced using the software Glitter (Van Achterbergh et al., 2001), and Isoplot-Ex (Ludwig, 2003) was used for age calculation. Uncertainty propagation was applied to the obtained data according to Horstwood et al. (2016).

4. Age

To constrain the age of the studied succession, U-Pb zircon dating was carried out on a tuff sample (Figs. 1, 2) by LA-ICP-MS. This rock is interlayered with distal delta front rhythmites in the upper portion of DS1, the basal unit of the IB (Figs. 1, 2). The tuff occurs near strata with MISS in outcrop M12 (Fig. 2). Approximately 70- to 250-μm-long zircon grains ($n = 35$) with prismatic and euhedral habits and sector zoning were extracted (Fig. 4A), following the work of Corfu et al. (2003). Juvenile igneous zircons (31 of 35 dated grains) were recognized, yielding a concordant age of 563 ± 3.3 Ma (95% confidence, MSWD = 1.6) (Fig. 4B), which corresponds to the magmatic crystallization age of the tuff.

These results broadly correlate this succession to the Avalon Assemblage (~570–557 Ma) (Schmitz, 2012; Noble et al., 2015; Pu et al., 2016) and mark the Itajaí Group as one of the earliest records of macroscopic life in Gondwana. The radiometric dating presented here is in accord with previously reported ages (Guadagnin et al., 2010), setting a minimal depositional age of 563 ± 3 Ma. Upper age limits given by the dating of the intrusive rhyolites that cross-cut the entire basin (ca. 558 Ma–549 Ma; Guadagnin et al., 2010; Basei et al., 2011) also corroborate an Avalonian age.

5. Body fossils

The body fossil assemblage includes *Palaeopascichnus*, *Aspidella*, *Nimbia*, and other problematic forms. These fossils were recovered from thin-bedded rhythmites related to upper slope (*Palaeopascichnus* and *Aspidella*) and distal delta front (*Aspidella* and *Nimbia*) depositional settings (Figs. 2, 3). The rhythmites are characterized by millimetric intercalations of clay and silt (Fig. 3B). The body fossils occur in association with abundant surface structures related to microbial mat growth in both slope and delta depositional environments. Additionally, neither body fossils nor MISS were found in the deeper facies (slope rise to basin plain).

Palaeopascichnus ($n = 27$) occurs as impressions comprising a series of straight to curved segments (i.e., chambers) and are abundantly preserved in some layers of mudstones in the thin-bedded rhythmite from outcrop A16 (Fig. 5). The chamber thickness varies from 0.1–0.3 mm, while the width varies from 0.3–1 mm. Some specimens show evidence of branching (Fig. 5A–B). The series width increases slightly in the direction of growth but diminishes after branching.

Palaeopascichnus is still considered to have unclear biological affinities, but it is well established as a body fossil (Antcliffe et al., 2011). Its chambered morphology has prompted previous comparisons with the modern group of giant protists Xenophyophora (Seilacher et al., 2003; Kolesnikov et al., 2018). Interestingly, this fossil is a long-ranging and, possibly, generalist organism (Kolesnikov et al., 2018), a common constituent of both the Avalon and White Sea Assemblages (Muscente et al., 2018), but also reported from deposits near the Ediacaran/Cambrian transition (Kolesnikov and Bobkov, 2019). Recent works have suggested that it may also represent one of the earliest skeletal (agglutinated) organisms (Kolesnikov et al., 2018). The presence of

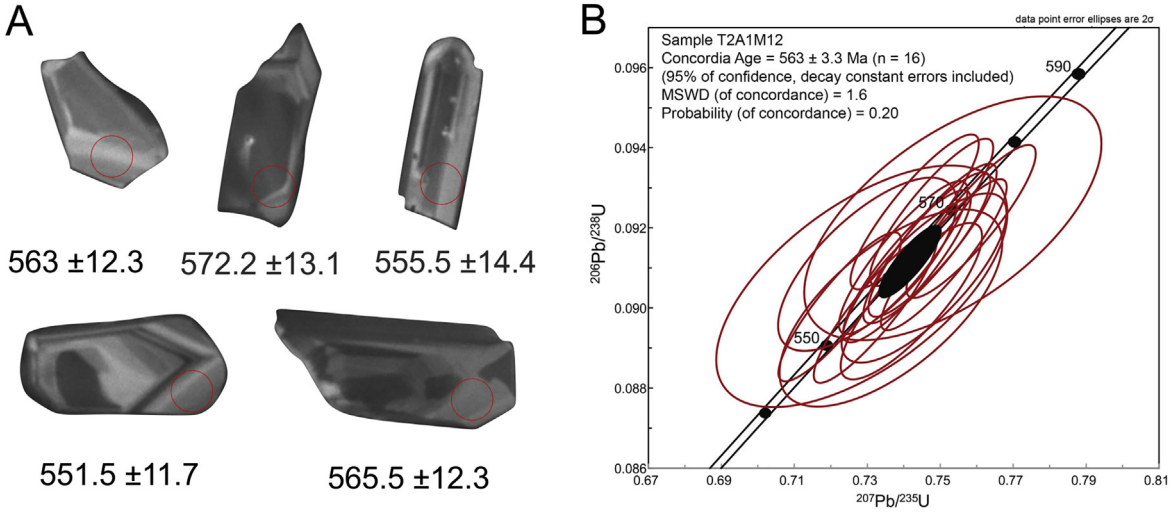

Fig. 4. A) Zircon morphologies obtained from the tuff investigated for radiometric U-Pb dating; B) Concordia diagram and concordia age obtained from the in situ LA-ICP-MS U-Pb zircon analyses.

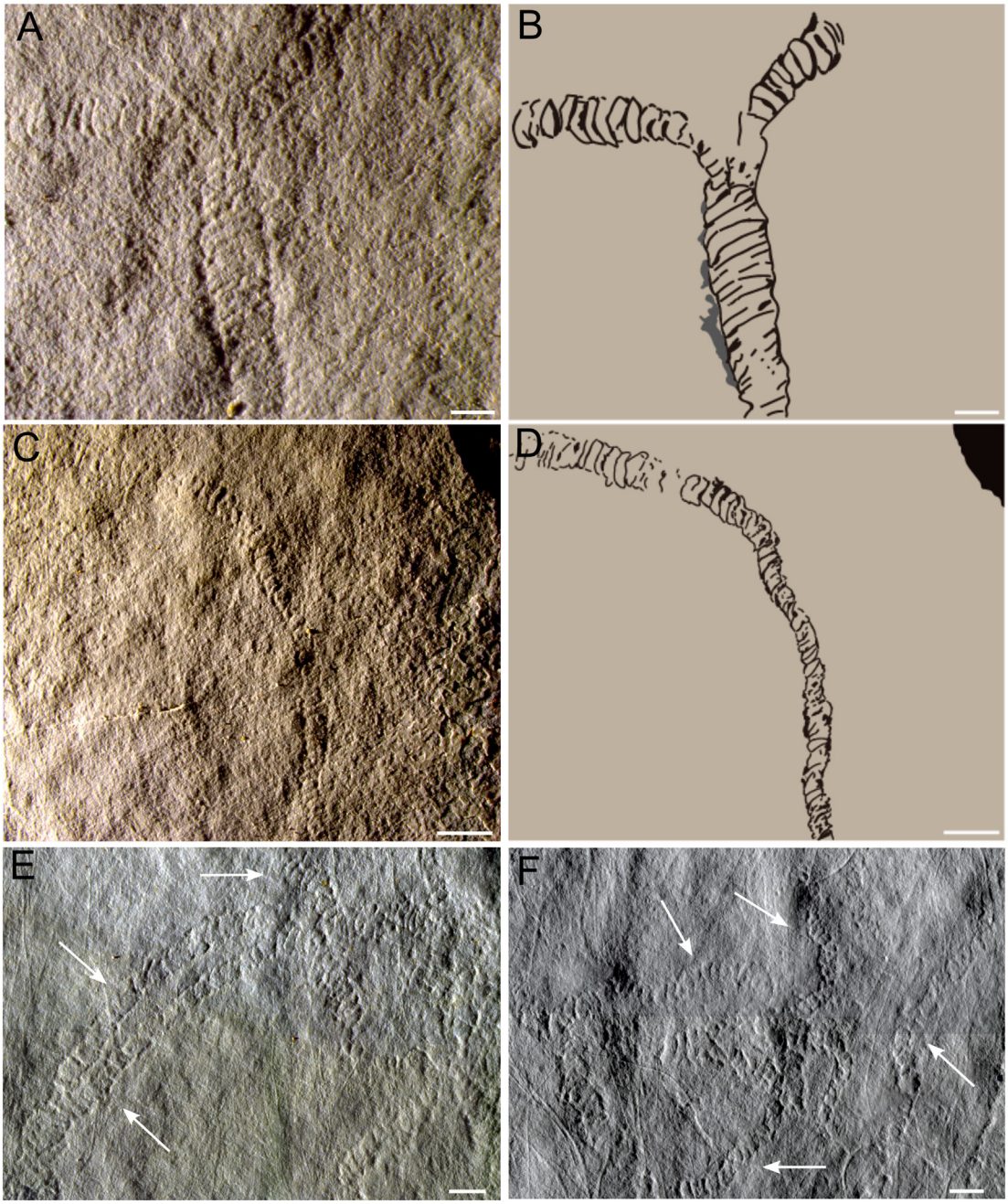

Fig. 5. *Palaeopascichnus* from the Itajaí Basin (CAP/1A–556). A) Specimen in positive epirelief showing bifurcation and a subsequent decrease in width; B) Interpretative drawing of A; C) Positive epirelief with *Palaeopascichnus* showing a gradual increase in width; D) Interpretative drawing of C. E–F) Several individuals occurring at the same level together with microbial filaments. Scales: 1 mm (A, B, E–F); 2 mm (C, D).

this fossil not only corroborates an Ediacaran age for the IB but also extends the paleobiogeographic range of this important taxon.

Aspidella specimens ($n = 11$) are preserved in negative to flat epirelief. These fossils mainly exhibit two morphotypes: convex and type morphs (following Gehling et al., 2000). The first morphotype is represented by convex ellipsoidal discs ($n = 4$) in positive hyporelief, with maximum diameters of ~10–14 mm and minimum diameters of ~9–12 mm. These forms present fine concave edges delimiting the convex disc. At the center, the disc shows a convex circular region (central boss) also delimited by a fine concave ring (Fig. 6A–B). One sample shows two conjoined specimens of the convex morph (Fig. 6C), while another presents an attached stalk-like structure (Fig. 6F–G). This morphotype was found within the thin-bedded rhythmite of outcrop A16 (upper slope setting). The type morphs (n = 4) were found in delta front and upper slope deposits and are preserved in negative epirelief; they are defined by an ellipsoidal disc (5–14 mm in diameter) with a concave external zone cut by radial lines that converge into a central ridge (Fig. 6D–E, H). Two of these specimens (Fig. 6H) were previously described as *Parvancorina* (Zucatti da Rosa, 2005). Additionally, two discs, similar to the intermediate forms described by Burzynski and Narbonne (2015), are characterized by faint ellipsoidal impressions with maximum diameters of 15–22 mm and minimum diameters of 10–17 mm (e.g., Fig. 6I).

Discoidal forms are one of the most common morphotaxa found in Ediacaran rocks, but there are also reports of similar fossils in rocks of different ages (Nagovitsin et al., 2008; Burzynski et al., 2020). Although usually regarded as the holdfasts of Ediacaran fronds (Gehling et al., 2000; Tarhan et al., 2015), other interpretations, including microbial

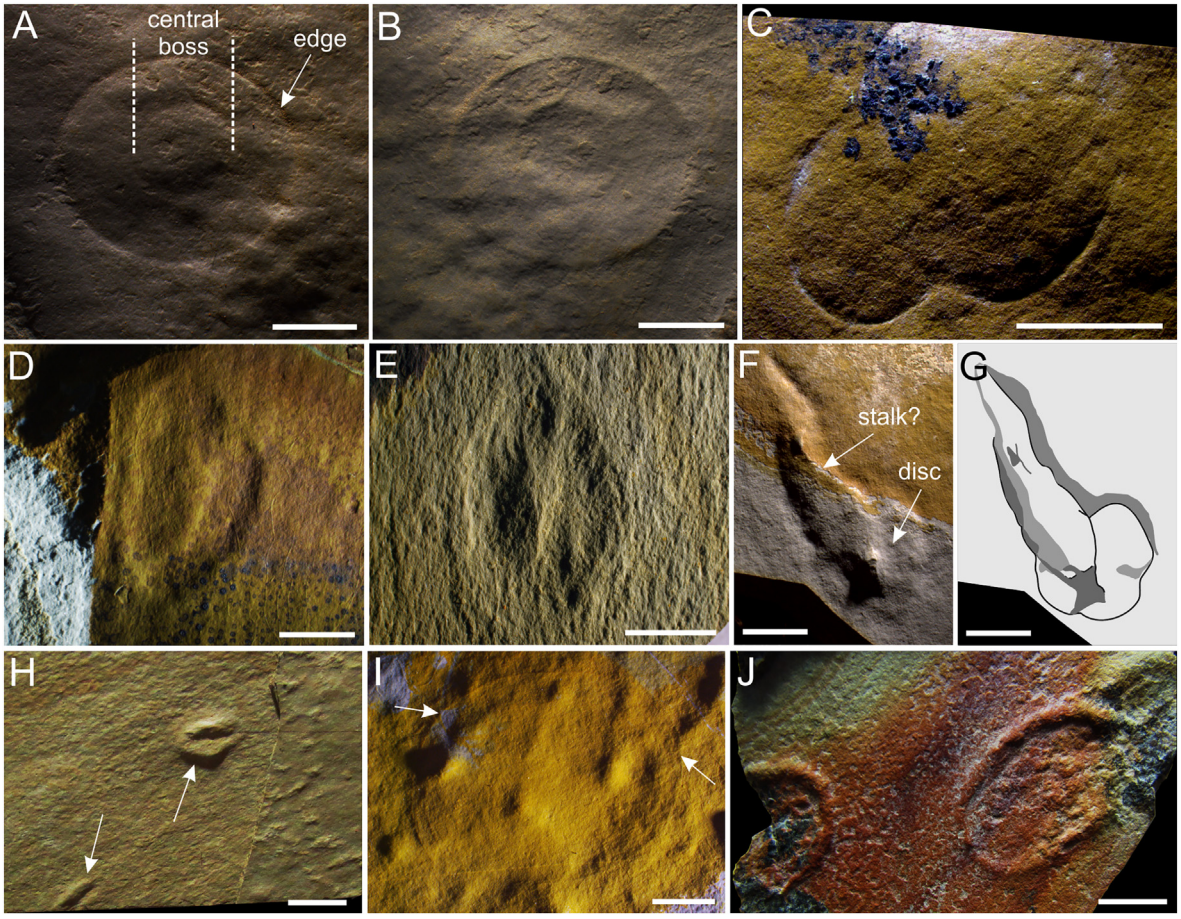

Fig. 6. Discoidal fossils from the Itajaí Basin. A) The convex morph of *Aspidella* in positive hyporelief, showing the central boss and concave edges (CAP/1A–549); B) counterpart of sample in (A). C) Conjoined specimens of the convex morph (CAP/1A–550); D–E) The type morph of *Aspidella* (arrows) from upper slope (D) and delta front deposits (E, H) (CAP/1A–878; CAP/1A–551); F) A disc (white arrow) in positive epirelief with possible attached stalk (black arrow) (CAP/1A–877); G) A schematic drawing of (F); H) Possible type morph of *Aspidella*, previously interpreted as *Parvancorina* (CAP/1A–552); I) Faint impression of a discoidal morphology (CAP/1A–555); J) *Nimbia* specimens from distal delta front deposits (CAP/1A–553). Scales: 5 mm (A–F, G, I); 10 mm (H, J, K).

colonies and fluid escape structures, have been made for some occurrences (Grazhdankin and Gerdes, 2007; Menon et al., 2016). Thus, studies dealing with discoidal impressions should evaluate these different possibilities. However, distinguishing the origin of these structures can be difficult, and several occurrences may still be considered problematic (e.g., Inglez et al., 2019).

In the IB, at least for the *Aspidella* morphs, our results showed that these fossils could be related to the basal portions of complex macroscopic forms (e.g., frondose organisms). For instance, one specimen preserved in positive epirelief showed an attached stalk-like structure (Fig. 6F–G) that could represent the stalk of a macroscopic frond-like organism. This structure greatly differs from the filamentous fossils described below, both by its larger size and tapered nature. Tool marks are an unlikely origin, since the observed feature is preserved in positive epirelief. Additionally, load casts were not seen in these beds, and their usual mode of occurrence (positive features on the sole of beds) differs from our case. Alternatively, another possibility is the formation by rolled-up mats, which could explain the positive epirelief of the structure. However, it is intriguing that this form appears to be associated with a disc.

Polished sections of *Aspidella* showed no evidence for fluid escape structures (Fig. 7). In some samples, convolute laminations are present, but an undisrupted layer of fine-grained sand just below the fossil suggests that the soft-sediment deformation had no influence on the morphology of the disc (Fig. 7C–D). Thus, it is unlikely that these forms represent fluid/gas escape features or abiotic geologic features. It is also questionable whether the fossils could represent microbial colonies, since they lack several concentric rings, sharp radially arranged furrows and filaments, all of which have been suggested to be evidence for a microbial colony origin (Grazhdankin and Gerdes, 2007).

In contrast to *Aspidella*, *Nimbia* ($n = 18$) is found only in the distal delta front deposits (outcrop AF236). These discoidal impressions are characterized by ellipsoidal rings in positive epirelief (Fig. 6J). The discs present major axes of 24–30 mm and minor axes of 16–19 mm, with annular ring widths of 1.5–3 mm. The annular ring surrounds a nearly flat surface, which presents only faint circular protrusions (Fig. 6J). One sample separated for thin sectioning did not exhibit fluid escape features or wavy-crinkly lamination.

Recent work (Liu et al., 2013) has suggested a microbial origin for *Nimbia*, an acceptable interpretation based on its similarity to modern ring structures constructed by the cyanobacteria *Lyngbya aestuarii* at Laguna Mormona (compare our Fig. 6J to Fig. 4E of Horodyski, 1977).

6. Three-dimensional microbial mats and MISS

6.1. Reticulated tufted mats

Most of the occurrences of microbially related structures represent reticulated tufted mats, which consist of millimetric pinnacles (or cones) connected by ridges (Fig. 8A–B). The centers of the pinnacles are circular to elliptical in horizontal sections (Fig. 8B, D), with a mean width of 1.7 mm ($n = 37$). The ridges present a mean width of 0.4 mm ($n = 37$) and are slightly larger in the proximities of the pinnacles and gradually decrease in width farther from them. These well-

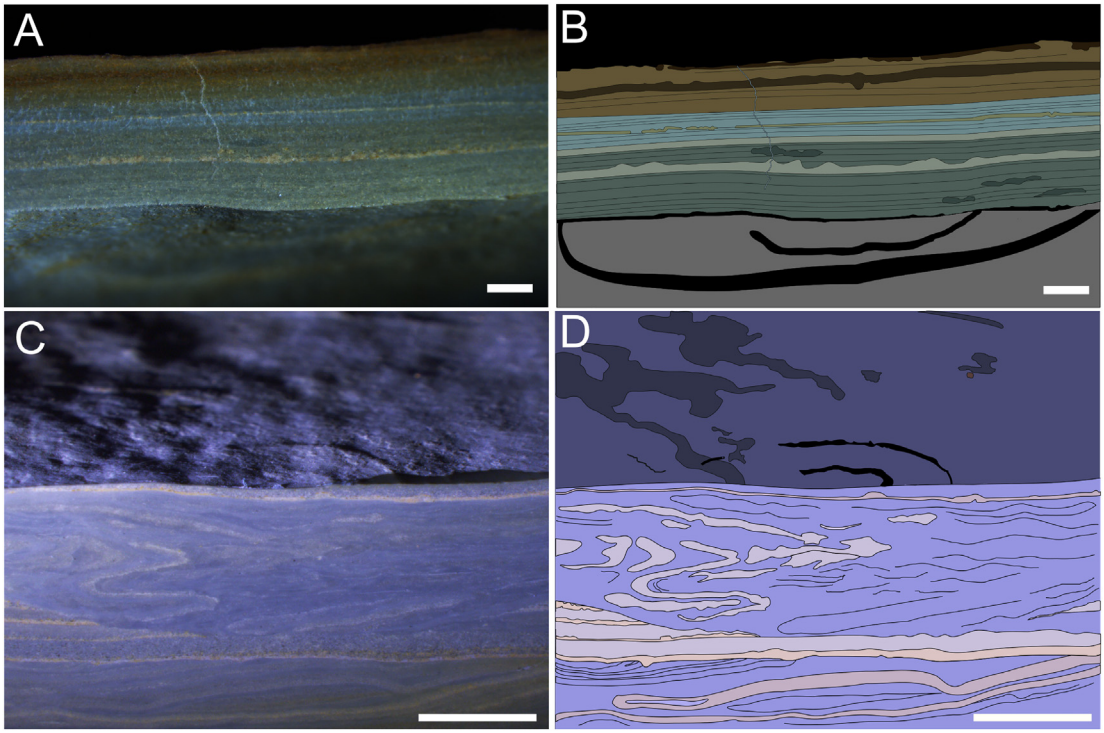

Fig. 7. Polished sections of *Aspidella*. A) Vertical section through positive hyporelief showing undisturbed laminations above the specimen; B) Schematic drawing of A; C) Section of epirelief demonstrating an undisturbed sandy layer below the specimen; D) Schematic drawing of C. Scales: 1 mm (A, B), 5 mm (C, D).

preserved tufted mats often co-occur with micrometric microbial filaments (Fig. 8E–F).

This type of microbial mat is abundant in the thin-bedded rhythmites (upper slope), where *Aspidella* and *Palaeopascichnus* also occur (outcrop A16), as well as in the distal delta front deposits. Specifically, in the upper slope facies, these fossilized tufted mats are three-dimensionally preserved, a feature clearly evident in polished and thin sections (Fig. 8B, D). The presence of Si, Al, K, Fe and Ti demonstrated by SR-μXRF point analysis (Supplementary Fig. 3) points to an aluminosilicate composition with associated titanium phases. In contrast, the tufted morphologies in the distal delta front deposits (Fig. 8G–I) are preserved only as impressions and are thus similar to the typical preservation of MISS.

Samples also show different degrees of interconnection of the centers. Small domes with incipient connections (Fig. 9A–B) gradually transition to more reticulated and interconnected mats (Fig. 10).

Wavy-crinkly laminae with evidence of cohesive behavior and disrupted laminations are also found associated with these tufts in thin sections (Fig. 9E–F). Horizontally oriented floating grains are observed within the wavy-crinkly laminations (Fig. 9G–H).

The three-dimensional preservation of the Itajaí Group reticulated mats has yielded good retention of the original morphology, apparently showing different degrees of developmental growth, from isolated domes through more interconnected samples to a fully established reticulated tufted mat (Fig. 9). Similar formative processes have been observed in recent photosynthetic reticulated mats (Shepard and Sumner, 2010). For instance, studies have associated the genesis of tufts and reticulated patterns with gradients in oxygen (Sim et al., 2012) and undirected filament gliding and collision, followed by their alignment and clumping (Shepard and Sumner, 2010). Conspicuously, the aforementioned processes of the origin and development of tufted mats (Walter et al., 1972, 1976; Flannery and Walter, 2012) may also account for the morphologies recorded in the Itajaí biota (Figs. 8–9). Additionally, it is worth noting that IB tufts are very similar to modern microbial tufts (see Fig. 2-1-4 in Schieber et al., 2007) constructed by filamentous cyanobacteria, such as *Lyngbya aestuarii* (Horodyski, 1977) and *Microcoleus chthonoplastes* (Schieber et al., 2007).

Likely due to the peculiar three-dimensional preservation (Fig. 8) of the tufted mats, these morphologies were first thought to represent the preserved remains of *Chancelloria* (Da Rosa et al., 1997; Leipnitz et al., 1997; Paim et al., 1997). However, the resemblance is only superficial since the IB structures do not present any boundaries related to a body outline, and the "sclerites" (i.e., pinnacles and ridges) lack the regular morphology observed in true *Chancelloria* sclerites. In contrast, these features cover the whole bedding plane surface and are irregular in the number of ridges that depart from the pinnacle.

Some variations in the morphology of these tufted mats can generate a false dumbbell appearance, which led to the interpretation of these features as the ichnogenus *Diplocraterion* (Netto and Zucatti da Rosa, 1997). However, we observed that these structures are characterized by millimetric domes interconnected by more than two strands (Fig. 10) and are similar in size to the reticulated microbial mats described above. Micro-computed tomography (μCT) analysis demonstrated no deformation in the laminations beneath the structures (Fig. 10C). This absence of *spreiten* morphologies in microtomographic investigations (Fig. 10C), combined with the interconnection of more than two spherical structures (Fig. 10D–E), suggests a network of interconnected tuft pinnacles and not a true dumbbell morphology related to a vertical shift in sediment.

The filamentous impressions occasionally occurring associated with the reticulated mats were also previously interpreted as trace fossils (i.e., *Helminthoidichnites*; Netto, 2012). Instead, our observations suggest that these fossils represent exquisitely preserved microbial filaments. Their body fossil nature is evident by the overlap of individuals (Fig. 8E–F), instead of a cross-cutting interaction that would be expected in horizontal trace fossils. For the same reason, these filaments are unlikely to be tectographs (e.g., Seilacher et al., 2000). Therefore, no strong evidence indicates the presence of ichnofossils in the IB – a situation that is similar to other deposits with analogous ages (but see references Liu et al., 2010 and Liu et al., 2015 for putative trace fossils in the

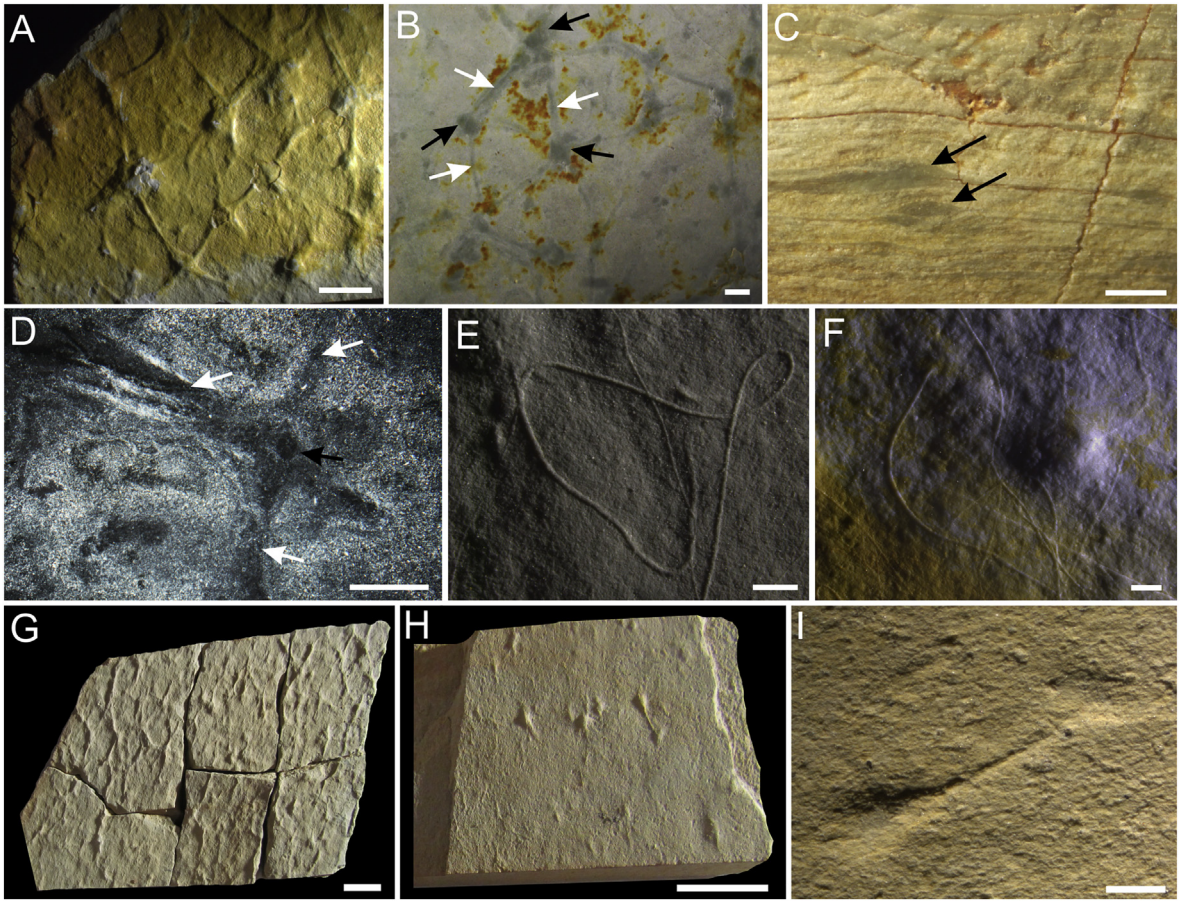

Fig. 8. Hand samples and thin sections of microbial tufted mats. A) Bedding plane views of three-dimensional microbial tufts (CAP/1A–559); B) Hand sample polished parallel to the bedding plane, revealing the preservation of the microbial mats by an argillaceous material darker than the surrounding rock (CAP/1F–03). Note the sectioned pinnacles (black arrows) and the ridges connecting them (white arrows) (CAP/1F–03); C) Transverse section of a hand sample, indicating the presence of small elevations that correspond to the cones of the mat (arrows) (CAP/1A–560); D) Thin sections made parallel to the bedding plane, highlighting the three-dimensional morphology of the microbial mats, with ridges (white arrows) and pinnacles (black arrows) (CAP/1F–03). (E–F) Micrometric filaments often found associated with the first stages of formation of the tufted mats (CAP/1A–561; CAP/1A–555). (G–I) Reticulated tufts preserved as simple surface morphologies (CAP/1A–570; CAP/1A–571). Scales: 5 mm (A); 1 mm (B–C, E–F, I); 0.5 mm (D); 10 mm (G, H).

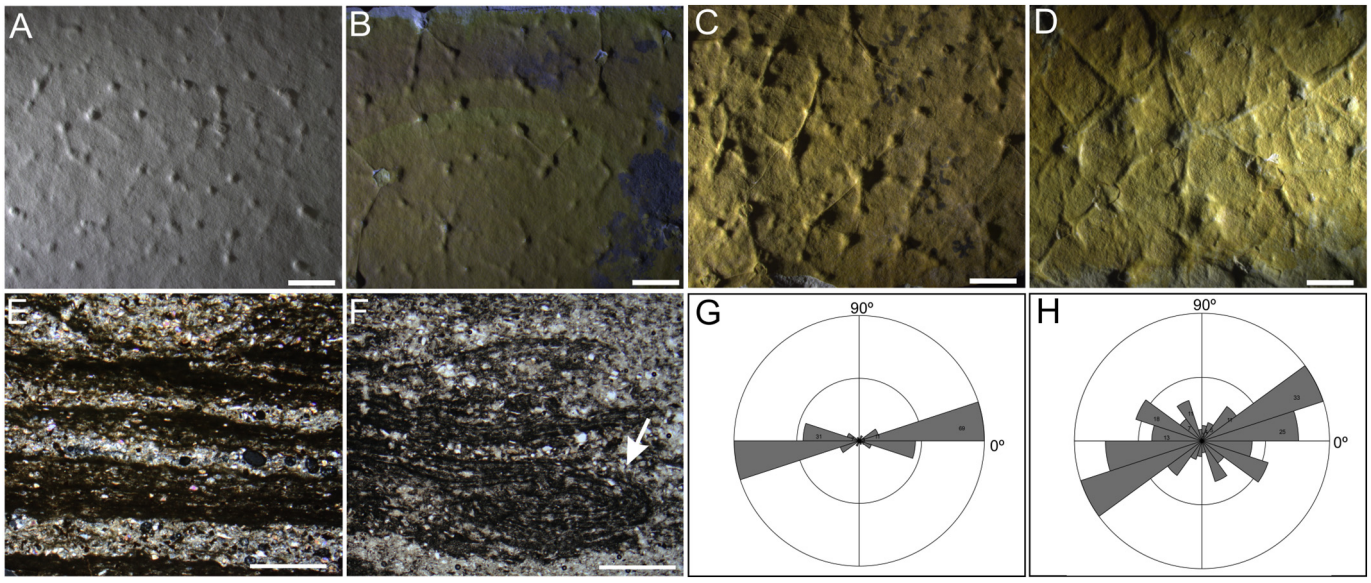

Fig. 9. Different stages of formation of tufted microbial mats (CAP/1A–567; CAP/1A–568; CAP/1A–569; CAP/1A–559). E–F) Wavy-crinkly lamination with abundant floating grains (CAP/1F–08), and evidence of soft deformation (B) (CAP/1F–09); G) Orientation of grains inside microbial laminae ($n = 125$); H) Orientation of grains in the siltstone-sandstone layers ($n = 130$). Scales: 5 mm. (A–E); 1 mm (E–F).

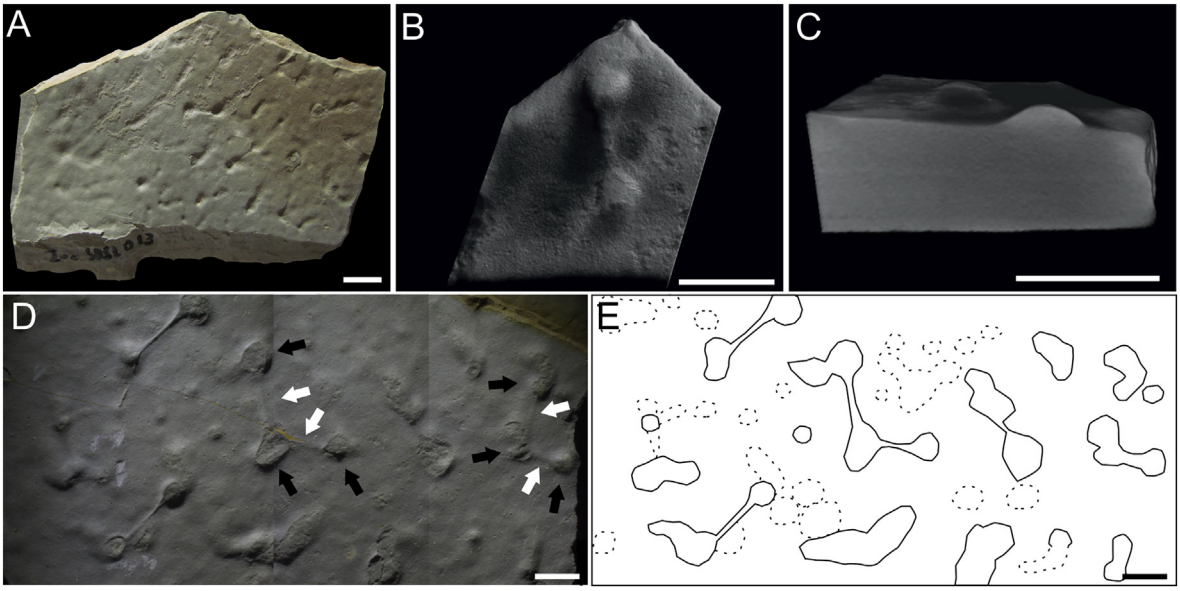

Fig. 10. Tufted microbial mats resembling dumbbell morphologies (CAP/1A–579). A) Hand sample with interconnected dumbbell forms; B) μCT image of the surface of a sample with a dumbbell shape; C) Transverse section of the μCT reconstruction; D) Hand sample demonstrating the presence of more than two spherical structures (black arrows) interconnected by strands (white arrows); E) Schematic representation of D. Scales: 10 mm (A); 5 mm (B–E).

Avalonian biota). Abundant and undisputable trace fossils appear later in the White Sea Assemblage (Droser et al., 2006).

6.2. Arumberia-type microbial mats

Another type of 3-D preservation of microbial mats in the Itajaí Group is Arumberia (Fig. 13). This fossil consists of an almost parallel series of filamentous structures arranged horizontally on the bedding planes (Fig. 11A–C). Lateral connections are observed. The width of the filaments can vary along stratigraphic levels, but they occur mainly in two size ranges: 0.5–0.8 mm (mean = 0.52, $n = 16$) and 0.9–3 mm (mean = 1.6, $n = 40$). Extremities are not observed, but dichotomous ramifications of the filaments are more abundant in the smaller type than in the larger one. Most of the structures are three-dimensionally preserved in a manner similar to that described above for the reticulated tufts (Fig. 11D), and thin sections indicate that the filaments exhibit ellipsoidal or domal outlines with convex tops in cross-section (Fig. 11D). The base of the mats presents a more horizontal surface than the top, apparently following the bedding plane (Fig. 11D). Arumberia appears both in the distal delta front and upper slope settings. Orientation measurements of Arumberia crests in the first depositional setting show a preferential direction (Supplementary Fig. 4) that is comparable to previously reported paleocurrent readings for the same depositional sequence (Fonseca, 2004).

The biological affinity of Arumberia is still considered controversial (Davies et al., 2016) since it has been interpreted as a body fossil (Glaessner and Walter, 1975), an abiogenic structure resulting from turbid flow (Brasier, 1979), and the product of scouring currents on a microbial mat surface (McIlroy and Walter, 1997). Our three-dimensional specimens preserved by aluminosilicates presenting laterally continuous connections in perpendicular sections corroborate a mat morphology, thus supporting the third interpretation.

Remarkably, the similar orientations between the crests of Arumberia (Supplementary Fig. 4) and sedimentary structures (Fonseca, 2004) in the delta front deposits of the IB indicate that currents indeed could have played a role in the formation of this peculiar morphology. Additionally, its occurrence in the delta front deposits suggests that this structure most likely represents the growth of photosynthetic microbial communities. Arumberia-like mats have recently been observed in modern photosynthetic mats (Kolesnikov et al., 2017).

6.3. Simple wrinkled surfaces

Simple wrinkles are the most common surface structures in the delta front and prodelta sediments of the IB (Fig. 11E–I). They are defined by simple reticulated textures formed by a network of intertwined convex ridges (0.2–1.8 mm). In contrast to the tufts, these wrinkles do not present either pinnacles or a more organized reticulated fabric. Some samples display rare associated submillimetric filaments (Fig. 11F). The hyporelief of the reticulated structures is characterized by convex bulbous polygons and narrow concave depressions, similar to the so-called elephant-skin texture. In transverse sections and thin sections, the wrinkles appear as crinkly laminations alternating with iron oxide-rich laminae (Fig. 11G–I). There are no significant changes in the grain size between the laminations.

These wrinkles are interpreted to represent surface sedimentary features related to mat growth, as evidenced by the crinkly laminae in thin sections and their resemblance to biolaminites in vertical sections (Fig. 11G–I). The origin by loading can be ruled out by the homogeneous grain size (mostly clay to fine-grained silt) at the interfaces where the wrinkles occur (Fig. 11I). Additionally, their association with putative microbial filaments (Fig. 11F) further supports a microbial mat interpretation. These simple wrinkles differ from the reticulated tufts by their more irregular arrangement and lack of pinnacles. It is unlikely that they represent a taphonomic variation of the latter because gradational morphologies were not observed and the presence of fine structures such as filaments suggests that some surfaces were relatively well preserved.

6.4. Small discoidal structures

Simple and abundant discoidal protrusions were observed on top of the beds (positive epirelief) in outcrop AF236 and near the Arumberia level, although the two are seldom seen in the same bedding plane. These 'pimples' exhibit circular to ellipsoidal outlines, millimetric diameters (1.2–3.7 mm), and heights of ca. 0.5 mm (Fig. 12). Some specimens show circular depressions in the center of the pimple (Fig. 12D), which is due to unequal partitioning of part and counterpart, leaving portions of the structure on the hyporelief (Fig. 12F). The counterparts (sole of the beds) are characterized by negative hyporelief circular impressions

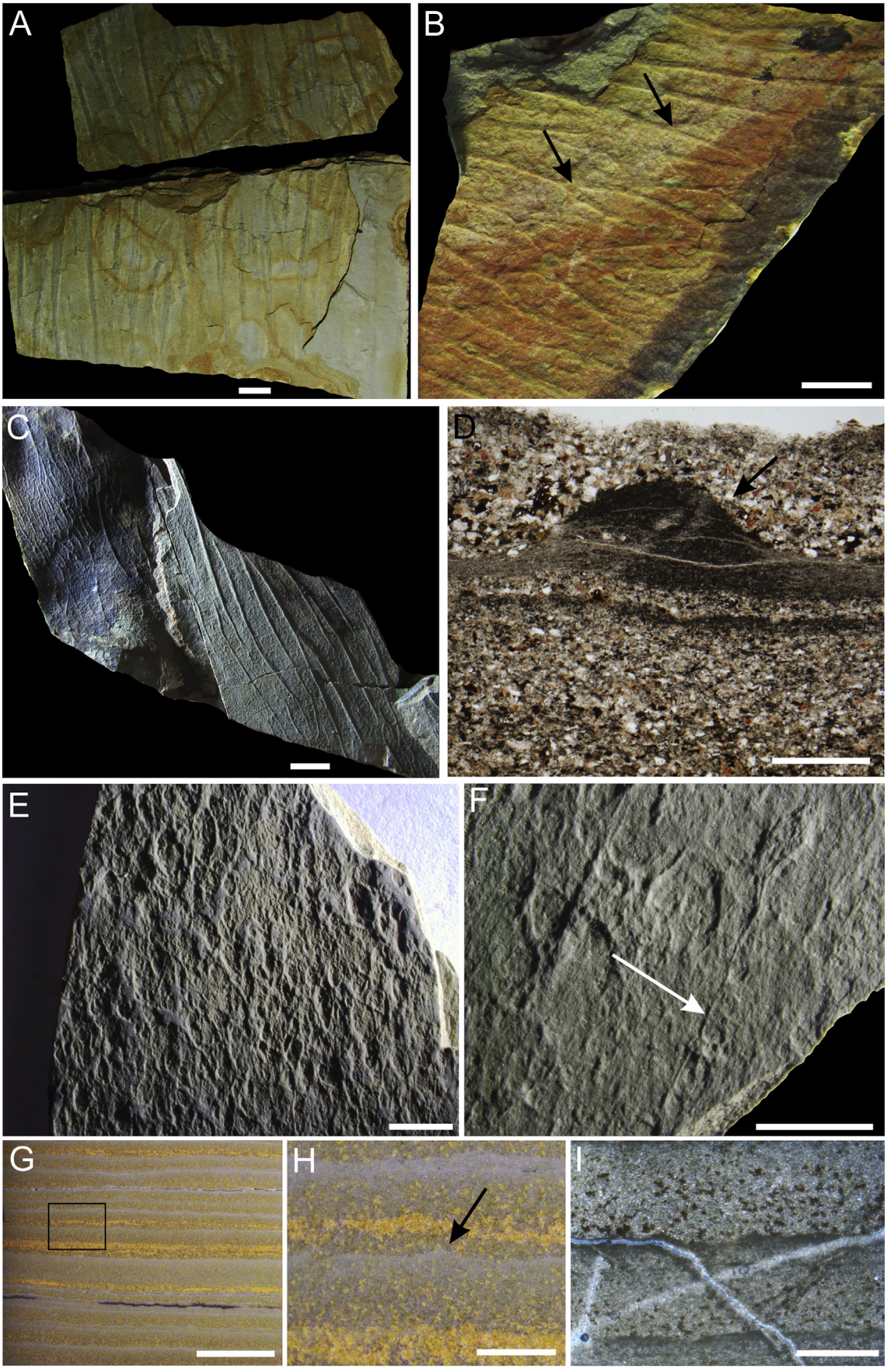
A
B
C
D
E
F
G
H
I

(Fig. 12F–G, K). Transverse sections of hand samples show no pipe or fluid escape structures, but some pimples present higher concentrations of clay minerals in the upper portion of the structure (Fig. 12H–I) or even in the whole pimple (Fig. 12I).

Simple and small discoidal structures are commonly observed in Meso-Neoproterozoic deposits (McIlroy et al., 2005; Callow et al., 2011; Menon et al., 2016), and a variety of taxonomic names (e.g., *Beltanelliformis brunsae*, *Beltanelliformis minutae*, *Intrites punctatus*, *Medusinites* aff. *asteroides*, and *Rameshia rampurensis*; see McIlroy et al., 2005 and Kumar and Pandey, 2008) or descriptive terms (e.g., small discoidal forms, mounds, domes, and pimples; see Menon et al., 2016 and Callow et al., 2011) have been used to encompass morphological variations of these forms. Thus, following the same pattern as for other discoidal impressions, controversies arise regarding their biological affinities. Recent works have presented strong evidence that some are the result of fluid escape and subordinate load structures, which occurred in a substrate dominated by microbial mats (Menon et al., 2016). In terms of morphology and size, IB small discs are more similar to the pimples reported by Menon et al. (2016) and Callow et al. (2011).

However, regarding the IB pimples, we did not observe pipes or disturbed laminations (Fig. 12H–K). Furthermore, they are preserved in positive epirelief, similar to the 1 Ga. pimples reported by Callow et al. (2011) but unlike the Ediacaran negative epirelief pimples of Menon et al. (2016). Strand connections observed between some IB specimens also argue against a fluid escape origin, suggesting similarities between the pimples and the stages of formation of microbial tufted mats. It is interesting to note that Arumberia is commonly reported to co-occur with small round impressions in positive epirelief (e.g., Bland, 1984; Kumar and Pandey, 2008; Callow et al., 2011; Kumar and Ahmad, 2014), as is the case in the IB. Therefore, we suggest that these forms represent different stages of formation of microbial surfaces and/or microbially bound surfaces under different energetic systems.

7. Problematic forms

7.1. Linearly arranged pits

These structures are characterized by impressions of serially arranged pits on the sole of the bed (negative hyporelief) (Fig. 13A–B). Each pit has a subrounded outline, and the diameter varies between 1 and 1.5 mm ($n = 10$). The distances between the centroids of each pit vary between 2.4 and 4.7 mm ($n = 8$). The specimen in Fig. 13A shows faint strings connecting the beads. One sample (CAP/1A-558) exhibits specimens preserved in three dimensions, possibly by iron oxides, as indicated by the higher intensities of Fe in the fossils than in the host matrix (Fig. 13D–G). In addition, there is displacement of sediment around one of the beads (Fig. 13C), suggesting formation prior to the lithification of the rock.

In contrast to other body fossils described here, the specimens described as linearly arranged pits are less discernable morphologically. However, their arrangement and the presence of strings connecting some of the circular structures (Fig. 13A) favor a biogenic origin. The morphology and size resemble those observed in the fossil *Horodyskia*. This taxon was defined as impressions of strings of beads, sometimes presenting connecting strands (Grey and Williams, 1990; Calver et al., 2010). However, *Horodyskia* has mostly been reported from Mesoproterozoic deposits, and Ediacaran occurrences, such as those in China (Shen et al., 2007; Dong et al., 2008) and India (Mathur and Srivastava, 2004), are considered controversial (Calver et al., 2010).

Alternatively, these linearly arranged pits could represent a different taphomorph of the pimples, in which bottom currents produced a linear arrangement of the structures. This could be the case for the sample illustrated in Fig. 13A but seems more unlikely for the 3-D forms considering their morphologies. In this sense, these two types of structures may exhibit distinct origins. The preservation by iron oxide also suggests that pyritization may have been the pathway for three-dimensional preservation. Nevertheless, due to an insufficient number of samples and poor preservation, no further interpretations about these structures can be made at present.

7.2. Stellate discs

Millimetric discs with submillimetric radial lines (Fig. 14) are present in two different preservation modes: as low relief molds and as flat yellow discs. In the first type, we observed displacement of sediment near the border of one of the discs. Stereomicroscopy and SEM investigations of the yellow discs showed the presence of cubic pseudomorphs of pyrite (Fig. 14G) and submicrometric star-shaped crystals, respectively (Fig. 15). EDS mapping demonstrated that the intensities of Fe are higher in the discoidal form than in the host rock (Fig. 14J–N).

Stellate discs similar to those in Fig. 14A–C were putatively interpreted as body fossils of the Cambrian taxon *Choia* (see Zucatti da Rosa, 2005; Becker-Kerber et al., 2015). However, the similarity of these forms with discoidal inorganic minerals (e.g., Seilacher, 2001) makes a biotic origin unlikely. For example, the displacement of sediment near the border of one of the specimens (Fig. 14C) is comparable to the structures that arise from the displacive growth of crystals (Seilacher, 2001). Additionally, the lobed arrangement of the radial grooves in our samples is also similar to the morphology of pyrite (or marcasite) discs (see Fig. 11a, b of Seilacher, 2001), also known as pyrite rosettes (Cloud, 1973), although other minerals can generate similar morphologies. Therefore, these IB discs are considered pseudofossils.

The yellow flat discs are even more likely to represent pseudomorphs after pyrite dissolution (Fig. 14D–I). These discs are similar to those preserved as molds in terms of their size and presence of radially oriented ridges and lobed edges. However, the yellow discs differ from the other forms by their flat nature and iron oxide composition (Fig. 15J–N). The nanometric star-shaped and acicular crystals found in SEM investigations (Fig. 15) corroborate this interpretation since these crystal habits are found in goethite and hematite (Cornell and Schwertmann, 2003). For instance, star-shaped crystals of goethite after marcasite and needles of the latter mineral have been reported filling the chambers of microfossils originally filled with organics (Soliman, 2001). The presence of submillimetric cubes associated with some specimens may also attest to a pyritic origin, as previously noted for other pseudofossils (Cloud, 1973). Hence, in the case of the stellate discs, the originally precipitated marcasite may have been pseudomorphosed into iron oxyhydroxides later in diagenesis. The same mechanism may account for the *Choia*-like molds, but in this case, the original mineral left no discernible geochemical traces.

The IB discs might have resulted from the activities of sulfate-reducing bacteria using some source of C_{org} and subsequently yielded the conditions for pyrite and/or marcasite precipitation (Southam et al., 2001). However, we acknowledge that at best, this interpretation is speculative since the validation of a microbial origin would require the study of isotopic fractionation in undissolved fresh discs.

Fig. 11. Arumberia mats and simple wrinkled surfaces. A–C) 3-D preserved specimens on a bedding plane (as viewed from above) exhibiting abundant linear crests and common ramifications (arrows) (CAP/1A–563; CAP/1A–564; CAP/1A–566); D) Thin section (in transmitted light) of a 3-D preserved Arumberia in transverse sections showing the domal outline of the crest and the lateral connections (CAP/1F–05). E–F) Hand samples with wrinkles on top of the beds (CAP/1A–572; CAP/1A–575). The white arrow highlights a filamentous structure; G) Transverse section and polished surface of a hand sample with wrinkles (CAP/1A–576); H) Enlargement of the rectangle in (C), presenting a ridge in cross-section (arrow); I) Thin section of wrinkles demonstrating little variation in grain size (mostly clay and fine silt) between the laminae. Scales: 10 mm (A–C); 0.5 mm (D); 5 mm (E–G); 1 mm (H–I).

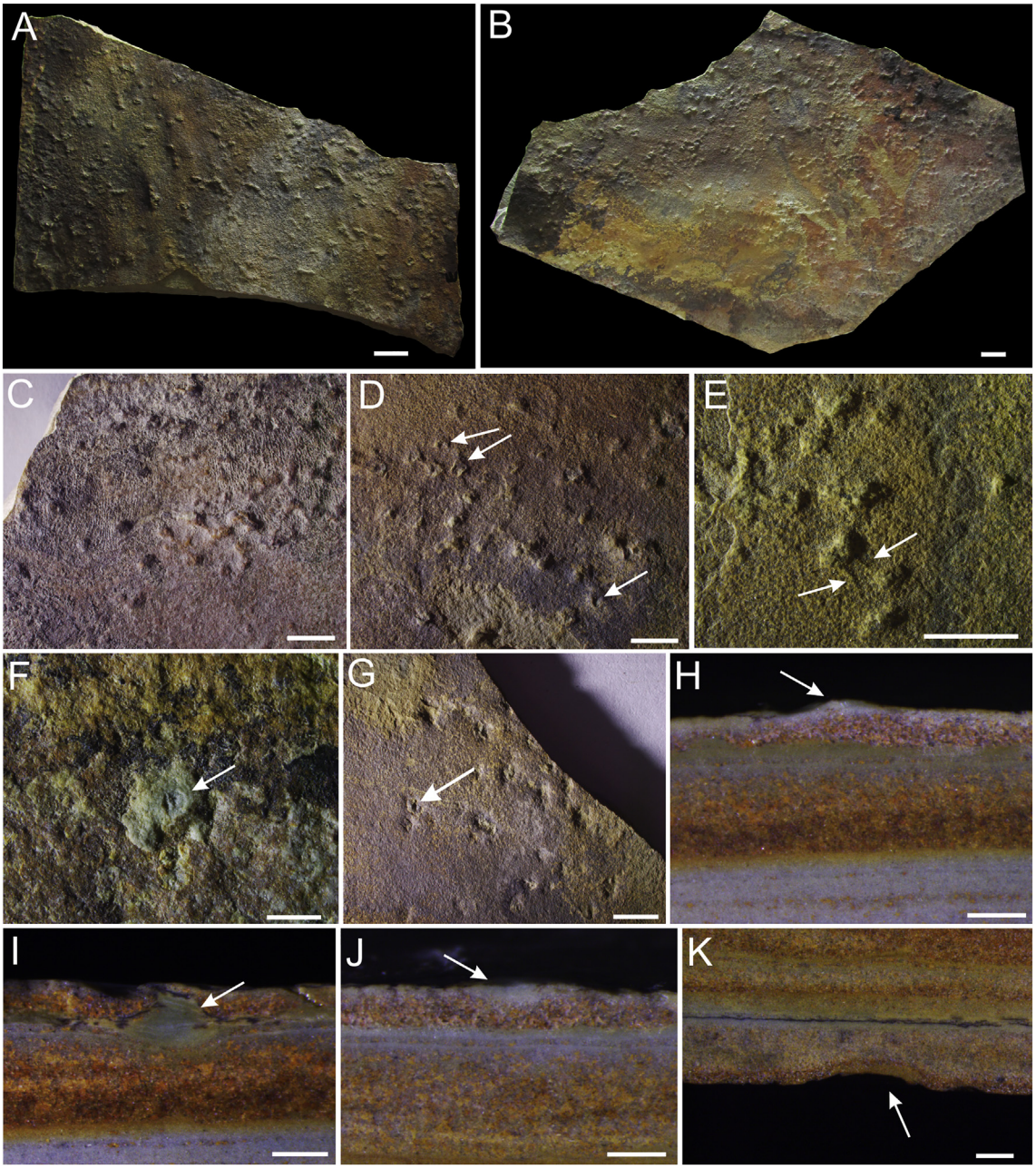

Fig. 12. Pimples from the Itajaí Basin. A–B) Hand samples with a profusion of specimens on top of the beds (positive epirelief) (CAP/1A–577; CAP/1A–578); C–E) Close-up of the structures in epirelief, showing depressions at the centers of some individuals (white arrows in D) and connecting ridges (white arrows in E) (CAP/1A–578); F) Portion of a pimple left on the bottom of the bed (CAP/1A–578); G) Hyporelief with small pits, corresponding to the counterpart of the pimple (CAP/1A–578). The white arrow marks the presence of portions of the pimple left behind after separation of the sample; H–J) Transverse sections of the pimples in epirelief (CAP/1A–577). Note the concentrations of argillaceous white material (white arrows). K. Transverse section of hyporelief (CAP/1A–577). Scales: 10 mm (A, B); 5 mm (C–E, G); 0.5 mm (F); 1 mm (H–K).

Interestingly, the size, shape, and preservation of the yellow discs are quite similar to problematic circular remains reported from intertillite beds of the Neoproterozoic Maikhanuul Formation (Serezhnikova et al., 2014), albeit the latter have been interpreted as being related to microbial colonies. This hypothesis is based mainly on the fact that the disc diameters are normally distributed and the discs are enriched in titanium and iron and bear nanometric particles that the authors described as "bacteriomorph structures" (Serezhnikova et al., 2014). However, it seems that some of the "bacteriomorph structures" represent the same crystal habit observed in the star-shaped nanocrystals reported here. Considering their Fe composition and similarity to the crystal habits of iron oxides, the Maikhanuul star-shaped submicrometric forms are also more parsimoniously interpreted as small crystals of goethite and/or hematite.

8. Discussion

8.1. The Ediacaran soft-bodied fossil record in South America

Deposits of Avalonian age bearing Ediacaran macrofossils are usually rare. Specifically, in South America, the Itajaí Group represents one of the earliest records of such a biota. Other Ediacaran fossil assemblages are generally more recent. For example, *Nemiana* was reported from the siliciclastic deposits of the Puncoviscana Formation in Argentina (Aceñolaza and Aceñolaza, 2007; Aceñolaza et al., 2009), but detailed studies employing polished sections to test other possible origins for these simple discs are lacking. In addition, Escayola et al. (2011) proposed an early Cambrian age for this unit, coeval with 540–535 Ma volcanic activity.

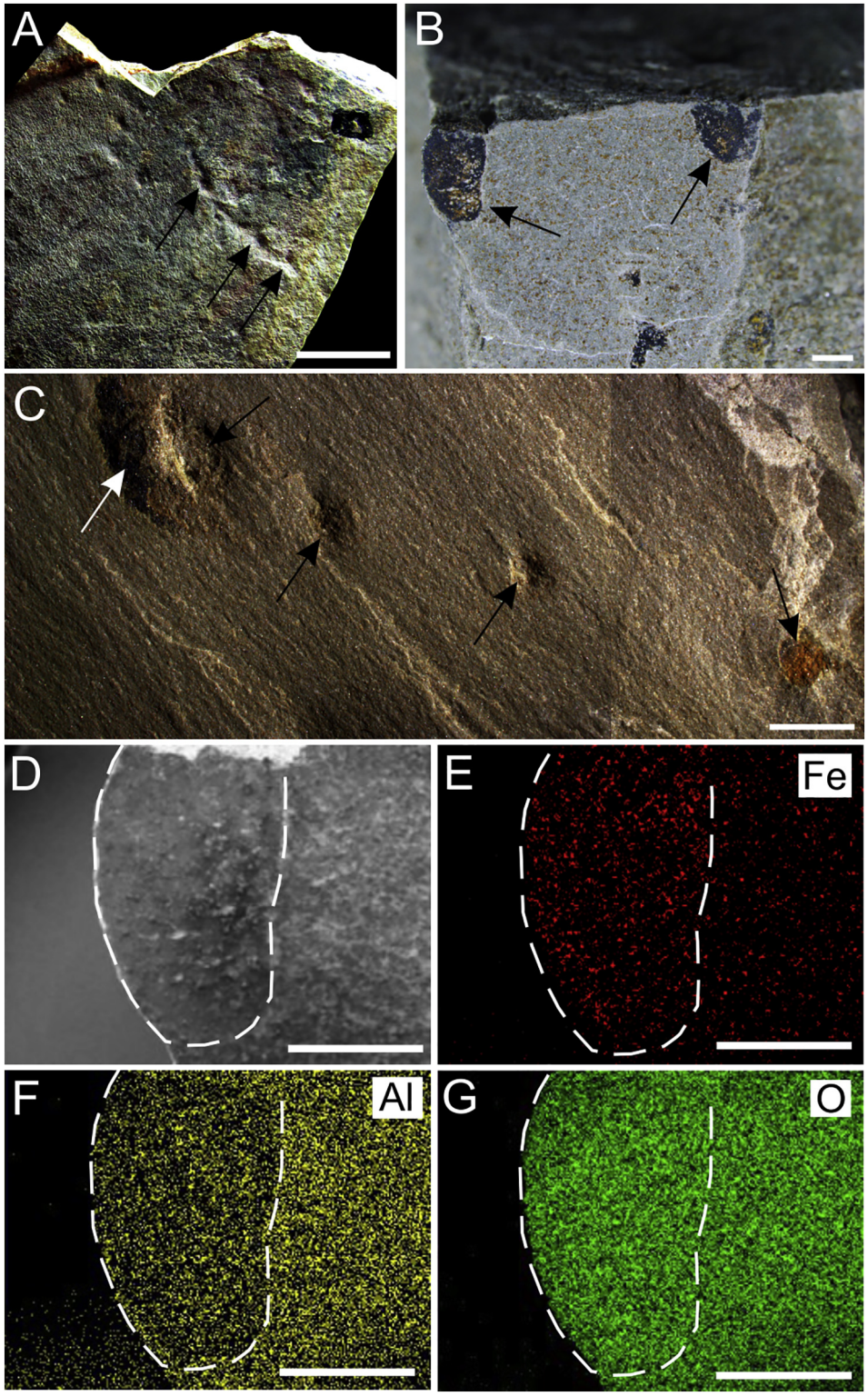

Fig. 13. Hand samples and energy-dispersive X-ray spectroscopy (EDS) maps of linearly arranged beads. (A) An impression of negative hyporelief of serially arranged pits (arrows) from the delta front deposits (CAP/1A–553). Note the presence of possible strings in the specimen; B–C) 3-D preservation of beads in transverse section (C) and in bedding plane view (D) (CAP/1A–558); D–G) Electron image (D) and EDS maps (E–G) of the specimen in (B). Scales: 10 mm (A); 1 mm (B, D–G); 5 mm (C).

Discoidal structures assigned to *Aspidella* have also been reported from the Cerro Negro Formation in Argentina (Arrouy et al., 2016), but these structures occur above deposits containing *Cloudina* fossils (Gaucher et al., 2005); hence, they are likely to be late Ediacaran to early Cambrian in age. Their interpretation as body fossils also requires further investigation (Inglez et al., 2019).

In Brazil, putative Ediacaran soft-bodied organisms have been described in siliciclastic rocks in the Jaibaras Basin (Barroso et al., 2014).

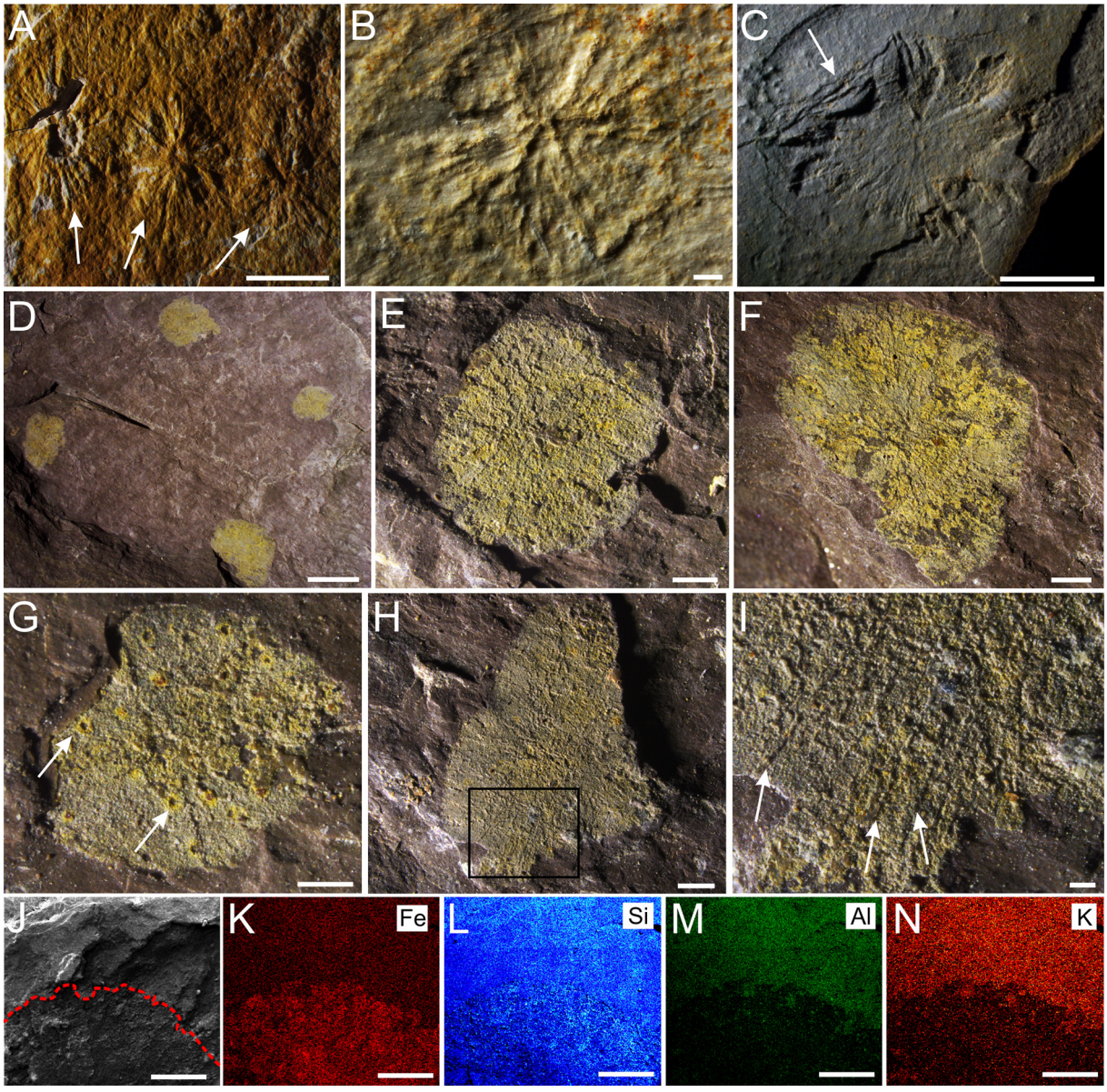

Fig. 14. Enigmatic discs from the IB. A. Three juxtaposed specimens of discs with radial lines (positive hyporelief) (CAP/1A–580). B. Radial disc with almost flat relief (CAP/1A–581). C. Irregular outline of one radial disc, with evidence of sediment displacement (white arrows) (CAP/1A–582). D–I. Flat, yellow discs with scarce radial crests (white arrows in I) and cubic crystals (white arrows in G) (CAP/1A–583). J–N) Electron image and EDS maps of a yellow disc (below the red line) (CAP/1A–584). Scales: 1 mm (B, E, F, H); 5 mm (A, C–D); 0.5 mm (G); 0.2 mm (I); 0.4 mm (J–N).

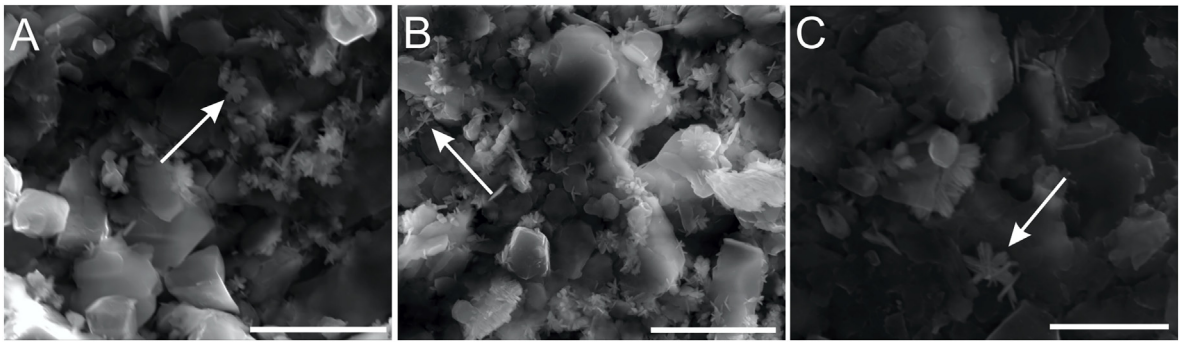

Fig. 15. A–B. Nanometric star-shaped and acicular crystals (white arrows) found in great abundance in the yellow discs from the IB (CAP/1A–584). C. Rare star-shaped crystals (white arrow) are also found in the rock matrix. Scales: 5 μm (A, B); 1 μm (C).

However, later reinterpretations of the geology and fossil content showed that the studied sections are part of the Silurian Ipu Formation (Parnaíba Basin, NE Brazil) (Barroso, 2016; Inglez et al., 2019). Consequently, these fossils are no longer considered to represent Ediacaran taxa (Barroso, 2016).

Finally, possible body fossils (*Aspidella*, *Intrites*, and *Sekwia*) have been described in the Camaquã Basin (southern Brazil), mostly in the ~559–540 Ma Santa Barbara Allogroup (Netto, 2012), with a maximum depositional age of 566 ± 6.9 Ma (Bicca et al., 2013). However, a microbial mat-influenced origin, such as that described by Menon et al. (2016), cannot be ruled out.

Therefore, the fossil assemblage reported here can be considered the oldest known Ediacaran biota in Gondwana and is associated with indisputable Ediacaran taxa. Although simple discoidal impressions in Ediacaran deposits do not always represent the holdfasts of large macroorganisms, the presence of *Palaeopascichnus* strongly corroborates the Ediacaran age of the deposits, broadening even further the paleobiogeographic occurrence of this important taxon.

8.2. The Itajaí Basin in the context of Ediacaran ecosystems

With the exception of a few claims of a shallow paleoenvironment for the Avalon biota (Retallack, 2016), several works have noted that these biological communities developed in deep-marine settings, well below the photic zone (Mason et al., 2013). This conclusion agrees with the scarcity of well-developed MISS in these deposits (Droser et al., 2017). The association of Ediacaran organisms with abundant MISS is well known in the younger White Sea and Nama Assemblages (Gehling and Droser, 2009; Droser et al., 2017), and they may even be involved in the moldic preservation of Ediacaran organisms, according to the death mask model (Gehling, 1999; Liu, 2016).

In contrast to the Avalonian record (Droser et al., 2017), the Itajaí biota occurs within strata that represent shallower conditions (delta front and upper slope deposits) and are also associated with abundant microbially influenced surfaces (Figs. 8–11). In particular, fossils of *Palaeopascichnus* and *Aspidella* found in thin-bedded rhythmites ascribed to an upper slope setting (outcrop A16) occur in association with abundant reticulated tufted mats (Figs. 8, 9). Moreover, it is important to note that both body fossils and microbial surfaces are absent in the deep basin plain deposits in the IB studied thus far. In this sense, the IB may help to understand the early colonization of shallower (distal delta front and upper slope) – possibly photic (abundant microbial tufted mats and MISS) – settings.

Some long-lasting taxa of Ediacaran macroscopic organisms, such as *Palaeopascichnus*, occur in Avalonian and White Sea deposits. This taxon not only had a widespread geographical distribution but possibly also adapted to very different environments: deep-marine and aphotic settings vs shallower and photic settings. Thus, understanding the ecological changes and/or bias in the geological record of the Ediacaran is fundamental to the development of a better picture of the early evolution of macroscopic life and its relation to environmental conditions. The IB offers a unique perspective regarding its age and depositional environments, with a macroscopic biota that, although depauperate, can record the early adaptations to shallower settings by probably generalist organisms such as *Palaeopascichnus*.

9. Conclusions

The IB can help to answer important open questions regarding the early evolution of macroscopic benthic communities during the Ediacaran Period. The IB fossil record provides evidence of the first steps of the colonization of shallower environments, possibly within the photic zone. The body fossil assemblage occurs in upper slope and distal delta front deposits associated with abundant and exquisitely preserved microbial mats, including the well-known Arumberia morphology. This situation differs from that observed in the deep-marine Avalonian deposits of Canada and England, where MISS are rarer. The discoidal impressions identified within the *Aspidella* plexus suggest the presence of frond-like macroorganisms. The remarkable presence of the indisputable Ediacaran taxon *Palaeopascichnus* further correlates the IB with the other Ediacaran deposits and, together with the radiometric dating (ca. 563 Ma), marks this unit as the oldest known occurrence of Ediacaran body fossils in Gondwana.

CRediT authorship contribution statement

Bruno Becker-Kerber: Conceptualization, Methodology, Investigation, Writing - original draft, Writing - review & editing, Visualization, Project administration. **Paulo Sergio Gomes Paim:** Conceptualization, Investigation, Writing - original draft, Writing - review & editing. **Farid Chemale Junior:** Investigation, Writing - original draft, Writing - review & editing, Visualization. **Tiago Jonatan Girelli:** Investigation, Writing - review & editing. **Ana Lucia Zucatti da Rosa:** Investigation, Writing - review & editing. **Abderrazzak El Albani:** Resources, Writing - review & editing. **Gabriel L. Osés:** Investigation, Writing - review & editing. **Gustavo M.E.M. Prado:** Investigation, Writing - review & editing. **Milene Figueiredo:** Investigation, Writing - review & editing. **Luiz Sérgio Amarante Simões:** Resources, Writing - review & editing. **Mírian Liza Alves Forancelli Pacheco:** Conceptualization, Writing - original draft, Writing - review & editing, Supervision, Funding acquisition.

Declaration of competing interest

The authors declare that they have no known competing financial interests or personal relationships that could have appeared to influence the work reported in this paper.

Acknowledgments

The authors are grateful for the support of the Fundação de Amparo à Pesquisa do Estado de São Paulo (FAPESP - Grant 2016/01827-4 and Grant 2018/21886-0), the Programa de Pós-Graduação em Ecologia e Recursos Naturais (PPGERN – UFSCar), and the Programa de Pós-Graduação em Geologia (PPGeo – UNISINOS). This work was also supported by La Région Nouvelle Aquitaine. We acknowledge C. Fontaine, C. Laforest for laboratory support at the University of Poitiers. The authors would like to thank the Brazilian Synchrotron Light Laboratory (LNLS-CNPEM) and the Brazilian Nanotechnology National Laboratory (LNNAno-CNEPM) for their technical support and for providing infrastructure for the SR-μXRF (proposal 20170438; 20171031), SEM/EDS (proposal 21836 and 23684) and μ-CT (proposal 20415) analyses. We also thank Petrobras Research Centre (CENPES) for all of their support with the palynological preparation, as well as the technical help of Igor Augusto Nascimento de Almeida and Gilton Braz de Aquino Filho. The authors are also grateful to Laboratório de Ecologia (UFMS), Alan Eriksson and Alêny Lopes Francisco Batista for enabling the stereomicroscope investigation. We thank the Laboratório de Preparação de Lâminas Delgadas of UNISINOS and the Setor de Laminação of UNESP (Rio Claro) for thin section preparation. We thank Fabiano Emmanuel Montoro for assistance with the SEM/EDS, and Gabriel Baréa Barros and Bianca Becker Kerber for their support in field activity. Finally, we would like to gratefully acknowledge all of the help we received from the citizens of Apiúna city during field investigations.

Appendix A. Supplementary data

Supplementary data to this article can be found online at https://doi.org/10.1016/j.gr.2020.03.007.

References

Aceñolaza, G.F., Aceñolaza, F.G., 2007. Insights in the Neoproterozoic–Early Cambrian transition of NW Argentina: facies, environments and fossils in the proto-margin of western Gondwana. Geological Society London Special Publications 286 (1), 1–13. https://doi.org/10.1144/SP286.1.

Aceñolaza, G.F., Germs, G.J.B., Aceñolaza, F.G., 2009. Trace fossils and the agronomic revolution at the Neoproterozoic-Cambrian transition in Southwest Gondwana. Developments in Precambrian Geology 16, 339–347. https://doi.org/10.1016/S0166-2635(09)01624-7.

Antcliffe, J.B., Gooday, A.J., Brasier, M.D., 2011. Testing the protozoan hypothesis for Ediacaran fossils: a developmental analysis of *Palaeopascichnus*. Palaeontology 54 (5), 1157–1175. https://doi.org/10.1111/j.1475-4983.2011.01058.x.

Arrouy, M.J., Warren, L.V., Quaglio, F., Poiré, D.G., Simões, M.G., Rosa, M.B., Peral, L.E.G., 2016. Ediacaran discs from South America: probable soft-bodied macrofossils unlock the paleogeography of the Clymene Ocean. Sci. Rep. 6 (30590). https://doi.org/10.1038/srep30590.

Barroso, F.R.G., 2016. Invertebrados fósseis da Formação Ipu (Siluriano), Grupo Serra Grande, Bacia do Parnaíba. (Doctorate thesis). Universidade Federal de Pernambuco, Recife.

Barroso, F.R.G., Viana, M.S.S., Filho, M.F., De, L., Agostinho, S.M.O., 2014. First Ediacaran fauna occurrence in Northeastern Brazil (Jaibaras Basin, ?Ediacaran-Cambrian): preliminary results and regional correlation. An. Acad. Bras. Cienc. 86 (3), 1029–1042. https://doi.org/10.1590/0001-3765201420130162.

Basei, M.A.S., Drukas, C.O., Nutman, A.P., Wemmer, K., Dunyi, L., Santos, P.R.D., Passarelli, C.R., Campos Neto, M.C., Siga, Jr.O., Osako, L., 2011. The Itajaí foreland basin: a tectono-sedimentary record of the Ediacaran period, Southern Brazil. Int. J. Earth Sci. 100 (2–3), 543–569. https://doi.org/10.1007/s00531-010-0604-4.

Becker-Kerber, B., Zucatti da Rosa, A.L., Paim, P.S.G., Pacheco, M.L.A.F., 2015. *Choia*-like impressions in ediacaran rocks (Itajaí Basin, Brazil) ?ecosystem engineers in shallow waters? Astrobioly Science Conference - Habitability, Habitable Worlds, and Life, 2015, Chicago Abstracts

Bicca, M.M., Chemale, Jr.F., Jelinek, A.R., de Oliveira, C.H.E., Guadagnin, F., Armstrong, R., 2013. Tectonic evolution and provenance of the Santa Bárbara Group, Camaquã Mines region, Rio Grande do Sul, Brazil. J. S. Am. Earth Sci. 48, 173–192. https://doi.org/10.1016/j.jsames.2013.09.006.

Blanco, G., Rajesh, H.M., Gaucher, C., Germs, G.J.B., Chemale, Jr.F., 2009. Provenance of the Arroyo del Soldado Group (Ediacaran to Cambrian, Uruguay): implications for the paleogeographic evolution of southwestern Gondwana. Precambrian Res. 171, 57–73. https://doi.org/10.1016/j.precamres.2009.03.003.

Bland, B.H., 1984. *Arumberia* Glaessner & Walter, a review of its potential for correlation in the region of the Precambrian–Cambrian boundary. Geol. Mag. 121, 625–633.

Boag, T.H., Darroch, S.A.F., Laflamme, M., 2016. Ediacaran distributions in space and time: testing assemblage concepts of earliest macroscopic body fossils. Paleobiology 42 (4), 574–594. https://doi.org/10.1017/pab.2016.20.

Boynton, H.E., Ford, T.D., 1995. Ediacaran fossils from the Precambrian (Charnian Supergroup) of Charnwood Forest, Leicestershire, England. Mercian Geol. 13, 165–182.

Brasier, M.D., 1979. The Cambrian radiation event. In: House, M.R. (Ed.), The Origin of the Major Invertebrate Groups. Academic Press, London, pp. 103–159.

Burzynski, G., Narbonne, G.M., 2015. The discs of Avalon: relating discoid fossils to frondose organisms in the Ediacaran of Newfoundland, Canada. Palaeogeogr. Palaeoclimatol. Palaeoecol. 434, 34–45. https://doi.org/10.1016/j.palaeo.2015.01.014.

Burzynski, G., Dececchi, T.A., Narbonne, G.M., Dalrymple, R.W., 2020. Cryogenian *Aspidella* from northwestern Canada. Precambrian Res. 336, 105507. https://doi.org/10.1016/j.precamres.2019.105507.

Callow, R.H., Battison, L., Brasier, M.D., 2011. Diverse microbially induced sedimentary structures from 1Ga lakes of the Diabaig Formation, Torridon Group, northwest Scotland. Sediment. Geol. 239 (3), 117–128. https://doi.org/10.1016/j.sedgeo.2011.06.002.

Calver, C.R., Grey, K., Laan, M., 2010. The 'string of beads' fossil (*Horodyskia*) in the mid-Proterozoic of Tasmania. Precambrian Res. 180 (1), 18–25. https://doi.org/10.1016/j.precamres.2010.02.005.

Cloud, P., 1973. Pseudofossils: a plea for caution. Geology 1 (3), 123–127. https://doi.org/10.1130/0091-7613(1973)1<123:PAPFC>2.0.CO;2.

Corfu, F., Hanchar, J.M., Hoskin, P.W.O., Kinny, P., 2003. Atlas of zircon textures. Rev. Mineral. Geochem. 53 (1), 469–500. https://doi.org/10.2113/0530469.

Cornell, R.M., Schwertmann, U., 2003. The Iron Oxides: Structure, Properties, Reactions, Occurrences and Uses. Wiley, Weinheim.

Da Rosa, A.A.S., Paim, P.S.G., Chemale Jr., F., Zucatti da Rosa, A.L., Girardi, R.V., 1997. The "state-of-art" of the Cambrian Itajaí Basin (Southern Brazil). 18th IAS Regional European Meeting of Sedimentology, Heidelberg, Germany, p. 112.

Davies, N.S., Liu, A.G., Gibling, M.R., Miller, R.F., 2016. Resolving MISS conceptions and misconceptions: a geological approach to sedimentary surface textures generated by microbial and abiotic processes. Earth Sci. Rev. 154, 210–246. https://doi.org/10.1016/j.earscirev.2016.01.005.

Dong, L., Xiao, S., Shen, B., Zhou, C., 2008. Silicified *Horodyskia* and *Palaeopascichnus* from upper Ediacaran cherts in South China: tentative phylogenetic interpretation and implications for evolutionary stasis. J. Geol. Soc. 165 (1), 367–378. https://doi.org/10.1144/0016-76492007-074.

Droser, M.L., Gehling, J.G., Jensen, S.R., 2006. Assemblage palaeoecology of the Ediacara biota: the unabridged edition? Palaeogeography, Palaeoclimatology, Palaeoecology 232 (2), 131–147. https://doi.org/10.1016/j.palaeo.2005.12.015.

Droser, M.L., Tarhan, L.G., Gehling, J.G., 2017. The rise of animals in a changing environment: global ecological innovation in the Late Ediacaran. Annual Review of Earth and Planetary Science 45, 593–617. https://doi.org/10.1146/annurev-earth-063016-015645.

Escayola, M.P., van Staal, C.R., Davis, W.J., 2011. The age and tectonic setting of the Puncoviscana Formation in northwestern Argentina: an accretionary complex related to Early Cambrian closure of the Puncoviscana Ocean and accretion of the Arequipa-Antofalla block. J. S. Am. Earth Sci. 32 (4), 438–459. https://doi.org/10.1016/j.jsames.2011.04.013.

Flannery, D.T., Walter, M.R., 2012. Archean tufted microbial mats and the Great Oxidation Event: new insights into an ancient problem. Aust. J. Earth Sci. 59 (1), 1–11. https://doi.org/10.1080/08120099.2011.607849.

Fonseca, M.M., 2004. Sistemas deposicionais e estratigrafia de sequências da Bacia do Itajaí, SC e detalhamento do Complexo Turbidítico de Apiúna. (Doctorate thesis). UNISINOS, São Leopoldo.

Ford, T.D., 1958. Pre-Cambrian fossils from Charnwood Forest. Proc. Yorks. Geol. Soc. 31, 211–217.

Gaucher, C., 2000. Sedimentology, palaeontology and stratigraphy of the Arroyo del Soldado Group (Vendian to Cambrian, Uruguay). Beringeria 26, 1–120.

Gaucher, C., 2018. The Ediacaran-Early Cambrian fossil record in Southwest Gondwana. In: Siegesmund, S., Basei, M.A.S., Oyhantçabal, P., Oriolo, S. (Eds.), Geology of Southwest Gondwana. Springer, Cham, pp. 543–560.

Gaucher, C., Poiré, D.G., Gómez Peral, L., Chiglino, L., 2005. Litoestratigrafía, bioestratigrafía y correlaciones de las sucesiones sedimentarias del Neoproterozoico-Cambrico del Cratón del Río de La Plata (Uruguay y Argentina). Lat. Am. J. Sedimentol. Basin Anal. 12, 145–160.

Gehling, J.G., 1999. Microbial mats in Terminal Proterozoic siliciclastics: Ediacaran death masks. Palaios 14, 40–57. https://doi.org/10.1144/pygs.53.3.237.

Gehling, J.G., Droser, M.L., 2009. Textured organic surfaces associated with the Ediacara biota in South Australia. Earth Sci. Rev. 96 (3), 196–206. https://doi.org/10.1016/j.earscirev.2009.03.002.

Gehling, J.G., Narbonne, G.M., Anderson, M.M., 2000. The first named Ediacaran body fossil, *Aspidella terranovica*. Palaeontology 43 (3), 427–456. https://doi.org/10.1111/j.0031-0239.2000.00134.x.

Glaessner, M., Walter, M.R., 1975. New Precambrian fossils from the Arumbera Sandstone, Northern Territory, Australia. Alcheringa 1, 59–69. https://doi.org/10.1080/03115517508619480.

Grazhdankin, D., 2004. Patterns of distribution in the Ediacaran biotas: facies versus biogeography and evolution. Paleobiology 30 (2), 203–221. https://doi.org/10.1666/0094-8373(2004)030<0203:podite>2.0.co;2.

Grazhdankin, D., Gerdes, G., 2007. Ediacaran microbial colonies. Lethaia 40 (3), 201–210. https://doi.org/10.1111/j.1502-3931.2007.00025.x.

Gresse, P.G., Chemale, Jr.F., Silva, L.C., Walraven, F., Hartmann, L.A., 1996. Late- to post-orogenic basins of the Pan-African-Brasiliano collision orogen in southern Africa and southern Brazil. Basin Res. 8, 157–171.

Grey, K., Williams, I.R., 1990. Problematic bedding-plane markings from the Middle Proterozoic manganese subgroup, Bangemall Basin, Western Australia. Precambrian Res. 46 (4), 307–327.

Grotzinger, J.P., Bowring, S.A., Saylor, B.Z., Kaufman, A.J., 1995. New biostratigraphic and geochronologic constraints on early animal evolution. Science 270, 598–604. https://doi.org/10.1126/science.270.5236.598.

Guadagnin, F., Chemale, Jr.F., Dussin, I.A., 2010. Depositional age and provenance of the Itajaí Basin, Santa Catarina State, Brazil: implications for SW Gondwana correlation. Precambrian Res. 180, 156–182. https://doi.org/10.1016/j.precamres.2010.04.002.

Hofmann, H.J., O'brien, S.J., King, A.F., 2008. Ediacaran biota on Bonavista Peninsula, Newfoundland, Canada. Journal of Paleontology 82, 1–36.

Horodyski, R.J., 1977. *Lyngbya* mats at Laguna Mormona, Baja California, Mexico: comparison with proterozoic stromatolites. J. Sediment. Res. 47 (3), 1305–1320. https://doi.org/10.1306/212F732E-2B24-11D7-8648000102C1865D.

Horstwood, M.S.A., Košler, J., Gehrels, G., Jackson, S.E., McLean, N.M., Paton, C., Pearson, N.J., Sircombe, K., Sylvester, P., Vermeesch, P., Bowring, J.F., Condon, D.J., Schoene, B., 2016. Community-derived standards for LA-ICP-MS U-(Th-)Pb geochronology - uncertainty propagation, age interpretation and data reporting. Geostand. Geoanal. Res. 40, 311–332. https://doi.org/10.1111/j.1751-908X.2016.00379.x.

Inglez, L., Warren, L.V., Okubo, J., Simões, M.G., Quaglio, F., Arrouy, M.J., Netto, R.G., 2019. Discs and discord: the paleontological record of Ediacaran discoidal structures in the south American continent. J. S. Am. Earth Sci. 89, 319–336. https://doi.org/10.1016/j.jsames.2018.11.023.

Jackson, S.E., Pearson, N.J., Griffin, W.L., Belousova, E.A., 2004. The application of laser ablation-inductively coupled plasma-mass spectrometry to in situ U–Pb zircon geochronology. Chem. Geol. 211, 47–69. https://doi.org/10.1016/j.chemgeo.2004.06.017.

Jaffey, A.H., Flynn, K.F., Glendenin, L.E., Bentley, W.C., Essling, A.M., 1971. Precision measurement of half-lives and specific activities of ^{235}U and ^{238}U. Physical Review C 4, 1889–1906. https://doi.org/10.1103/PhysRevC.4.1889.

Kolesnikov, A.V., Bobkov, N.I., 2019. Revisiting the age of the Asha Group in the South Urals. Estud. Geol. 75 (2), e103.

Kolesnikov, A.V., Danelian, T., Gommeaux, M., Maslov, A.V., Grazhdankin, D.V., 2017. Arumberiamorph structure in modern microbial mats: implications for Ediacaran palaeobiology. Bulletin de la Société géologique de France 188 (1–2), 1–10 (doi: 0.1051/bsgf/2017006).

Kolesnikov, A.V., Rogov, V.I., Bykova, N.V., Danelian, T., Clausen, S., Maslov, A.V., Grazhdankin, D.V., 2018. The oldest skeletal macroscopic organism *Palaeopascichnus linearis*. Precambrian Res. 316, 24–37. https://doi.org/10.1016/j.precamres.2018.07.017.

Kumar, S., Ahmad, S., 2014. Microbially induced sedimentary structures (MISS) from the Ediacaran Jodhpur Sandstone, Marwar Supergroup, western Rajasthan. J. Asian Earth Sci. 91, 352–361.

Kumar, S., Pandey, S.K., 2008. Note on the occurrence *Arumberia banksi* and associated fossils from the Neoproterozoic Maihar Sandstone, Marwar Supergroup, Vindhyan Supergroup, Central India. J. Palaeontol. Soc. India 53 (1), 83–97.

Leipnitz, I.I., Paim, P.S.G., da Rosa, A.A.S., Zucatti da Rosa, A.L., Nowatzki, C.H., 1997. Primeira ocorrência de Chancelloriidae no Brasil. Congresso Brasileiro de Paleontologia, São Pedro, SP, Brasil 15.

Liu, A.G., 2016. Framboidal pyrite shroud confirms the 'death mask' model for moldic preservation of Ediacaran soft-bodied organisms. Palaios 31, 259–274. https://doi.org/10.2110/palo.2015.095.

Liu, A.G., McIlroy, D., Brasier, M.D., 2010. First evidence for locomotion in the Ediacara biota from the 565 Ma Mistaken Point Formation, Newfoundland. Geology 38 (2), 123–126. https://doi.org/10.1130/G30368.1.

Liu, A.G., Brasier, M.D., Bogolepova, O.K., Raevskaya, E.G., Gubanov, A.P., 2013. First report of a newly discovered Ediacaran biota from the Irkineeva Uplift, East Siberia. Newsl. Stratigr. 46 (2), 95–110. https://doi.org/10.1127/0078-0421/2013/0031.

Liu, A.G., Kenchington, C.G., Mitchell, E.G., 2015. Remarkable insights into the paleoecology of the Avalonian Ediacaran macrobiota. Gondwana Research 27 (4), 1355–1380 (doi: 0.1016/j.gr.2014.11.002).

Ludwig, K.R., 2003. User's Manual for Isoplot/Ex version 3.00—A Geochronology Toolkit for Microsoft Excel, N° 4. Berkeley Geochronology Center Special Publication, Berkley.

Mason, S.J., Narbonne, G.M., Dalrymple, R.W., O'Brien, S.J., 2013. Paleoenvironmental analysis of Ediacaran strata in the Catalina Dome, Bonavista Peninsula, Newfoundland. Can. J. Earth Sci. 50, 197–212. https://doi.org/10.1139/cjes-2012-0099.

Mathur, V.K., Srivastava, D.K., 2004. Record of tissue grade colonial eucaryote and microbial mat associated with Ediacaran fossils in Krol Group, Garhwal Syncline, lesser Himalaya, Uttaranchal. J. Geol. Soc. India 63, 100–102.

McIlroy, D., Walter, M.R., 1997. A reconsideration of the biogenicity of *Arumberia banksi* Glaessner & Walter. Alcheringa 21 (1), 79–80. https://doi.org/10.1080/03115519708619187.

McIlroy, D., Crimes, T.P., Pauley, J.C., 2005. Fossils and matgrounds from the Neoproterozoic Longmyndian Supergroup, Shropshire, UK. Geol. Mag. 142, 441–455. https://doi.org/10.1017/S0016756805000555.

Menon, L.R., McIlroy, D., Liu, A.G., Brasier, M.D., 2016. The dynamic influence of microbial mats on sediments: fluid escape and pseudofossil formation in the Ediacaran Longmyndian Supergroup, UK. J. Geol. Soc. 173 (1), 177–185. https://doi.org/10.1144/jgs2015-036.

Misra, S.B., 1969. Late Precambrian (?) fossils from southeastern Newfoundland. Geol. Soc. Am. Bull. 80, 2133–2140.

Muscente, A.D., Boag, T.H., Bykova, N., Schiffbauer, J.D., 2018. Environmental disturbance, resource availability, and biologic turnover at the dawn of animal life. Earth Sci. Rev. 177, 248–264. https://doi.org/10.1016/j.earscirev.2017.11.019.

Nagovitsin, K.E., Grazhdankin, D.V., Kochnev, B.B., 2008. Ediacaria in the Siberian hypostratotype of the Riphean. Dokl. Earth Sci. 419A, 423–427.

Narbonne, G.M., Gehling, J.G., 2003. Life after snowball: the oldest complex Ediacaran fossils. Geology 31, 27–30. https://doi.org/10.1130/0091-7613(2003)031%3C0027:LASTOC%3E2.0.CO;2.

Narbonne, G.M., Laflamme, M., Trusler, P.W., Dalrymple, R.W., Greentree, C., 2014. Deep-water Ediacaran fossils from Northwestern Canada: taphonomy, ecology, and evolution. J. Paleontol. 88, 207–223. https://doi.org/10.1666/13-053.

Netto, R.G., 2012. Evidences of life in terminal Proterozoic deposits of southern Brazil: a synthesis. In: Netto, R.G., Carmona, N.B., FMW, Tognoli (Eds.), Ichnology of Latin America - Selected Papers. Monografias da Sociedade Brasileira de Paleontologia, Porto Alegre.

Netto, R.G., Zucatti da Rosa, A.L., 1997. Registro icnofossilífero da Bacia do Itajaí, SC: Uma primeira visão. Congresso Brasileiro de Paleontologia, São Pedro, SP, Brasil 15.

Noble, S.R., Condon, D.J., Carney, J.N., Wilby, P.R., Pharaoh, T.C., Ford, T.D., 2015. U-Pb geochronology and global context of the Charnian Supergroup, UK: Constraints on the age of key Ediacaran fossil assemblages. GSA Bull. 127 (1–2), 250–265. https://doi.org/10.1130/B31013.1.

Paim, P.S.G., Leipnitz, I., Da Rosa, A.A.S., Zucatti da Rosa, A.L., 1997. Preliminary report on the occurrence of *Chancelloria* sp. in the Itajaí Basin, Southern Brazil. Revista Brasileira de Geociências 27 (3), 303–308.

Paim, P.S.G., Chemale, Jr.F., Lopes, R.C., 2000. A bacia do Camaquã. In: Holz, M., De Ros, L.F. (Eds.), Geologia do Rio Grande do Sul. CIGO/UFRGS, Porto Alegre.

Pu, J.P., Bowring, S.A., Ramezani, J., Myrow, P., Raub, T.D., Landing, E., Mills, A., Hodgin, E., Macdonald, F.A., 2016. Dodging snowballs: Geochronology of the Gaskiers glaciation and the first appearance of the Ediacaran biota. Geology 44 (11), 955–958. https://doi.org/10.1130/G38284.1.

Retallack, G.J., 2016. Ediacaran sedimentology and paleoecology of Newfoundland reconsidered. Sediment. Geol. 333 (15), 15–31. https://doi.org/10.1016/j.sedgeo.2015.12.001.

Rostirolla, S.P., 1991. Tectônica e Sedimentação da Bacia do Itajaí – SC. (Masters dissertation). UFOP, Ouro Preto.

Rostirolla, S.P., Alckmin, F.F., Soares, P.C., 1992. O Grupo Itajaí, Estado de Santa Catarina, Brasil: Exemplo de sedimentação em uma bacia flexural de antepaís. Boletim de Geociências da Petrobrás 6 (3/4), 109–122.

Santos, M.M., Lana, C., Scholz, R., Buick, I., Schmitz, M.D., Kamo, S.L., Gerdes, A., Corfu, F., Tapster, S., Lancaster, P., Storey, C.D., Basei, M.A.S., Tohver, E., Alkmim, A., Nalini, H., Krambrock, K., Fantini, C., 2017. A new appraisal of Sri Lankan BB Zircon as a reference material for LA-ICP-MS U-Pb Geochronology and Lu-Hf Isotope Tracing. Geostand. Geoanal. Res. 41 (3), 335–358. https://doi.org/10.1111/ggr.12167.

Saylor, B.Z., Grotzinger, J.P., Germs, G.J.B., 1995. Sequence stratigraphy and sedimentology of the Neoproterozoic Kuibis and Schwarzrand Subgroups (Nama Group), southwestern Namibia. Precambrian Res. 73, 153–171. https://doi.org/10.1016/0301-9268(94)00076-4.

Schieber, J., Bose, P.K., Eriksson, P.G., Banerjee, S., Sarkar, S., Altermann, W., Catuneanu, O., 2007. Atlas of Microbial Mat Features Preserved Within the Siliciclastic Rock Record. vol. 2. Elsevier, Amsterdam 9780444528599 324 p.

Schmitz, M.D., 2012. Appendix 2: radiometric ages used in GTS2012. In: Gradstein, F., Ogg, J., Schmitz, M.D., Ogg, G. (Eds.), The Geologic Time Scale 2012. Elsevier, Boston.

Seilacher, A., 2001. Concretion morphologies reflecting diagenetic and epigenetic pathways. Sediment. Geol. 143 (1), 41–57. https://doi.org/10.1016/S0037-0738(01)00092-6.

Seilacher, A., Meschede, M., Bolton, E.W., Luginsland, H., 2000. Precambrian 'fossil' Vermiforma is a tectograph. Geology 28, 235–238.

Seilacher, A., Grazhdankin, D., Legouta, A., 2003. Ediacaran biota: the dawn of animal life in the shadow of giant protists. Paleontological research 7 (1), 43–54. https://doi.org/10.2517/prpsj.7.43.

Serezhnikova, E.A., Ragozina, A.L., Dorjnamjaa, D., Lyubov'V, Z., 2014. Fossil microbial communities in Neoproterozoic interglacial rocks, Maikhanuul formation, Zavkhan basin, Western Mongolia. Precambrian Res. 245, 66–79. https://doi.org/10.1016/j.precamres.2014.01.005.

Shen, B., Xiao, S., Dong, L., Zhou, C., Liu, J., 2007. Problematic macrofossils from Ediacaran successions in the North China and Chaidam blocks: implications for their evolutionary roots and biostratigraphic significance. J. Paleontol. 81 (6), 1396–1411. https://doi.org/10.1666/06-016R.1.

Shen, B., Dong, L., Xiao, S., Kowalewski, M., 2008. The Avalon explosion: evolution of Ediacara morphospace. Science 319 (5859), 81–84. https://doi.org/10.1126/science.1150279.

Shepard, R.N., Sumner, D.Y., 2010. Undirected motility of filamentous cyanobacteria produces reticulate mats. Geobiology 8, 179–190. https://doi.org/10.1111/j.1472-4669.2010.00235.x.

Sim, M.S., Liang, B., Petroff, A.P., Evans, A., Klepac-Ceraj, V., Flannery, D.T., Walter, M., Bosak, T., 2012. Oxygen-dependent morphogenesis of modern clumped photosynthetic mats and implications for the Archean stromatolite record. Geosciences 2 (4), 235–259. https://doi.org/10.3390/geosciences2040235.

Sláma, J., Kosler, J., Condon, D.J., Crowley, J.L., Gerdes, A., Hanchar, J.M., Horstwood, M.S.A., Morris, G.A., Nasdala, L., Norberg, N., Schaltegger, U., Schoene, B., Tubrett, M.N., Whitehouse, M.J., 2008. Plešovice zircon — a new natural reference material for U–Pb and Hf isotopic microanalysis. Chem. Geol. 249, 1–35. https://doi.org/10.1016/j.chemgeo.2007.11.005.

Soliman, M.F., 2001. The mineralogy and geochemistry of the Paleocene succession at Gabal El-Qreiya, Nile Valley, Egypt. The Second International Conference on the Geology of Africa, Assiut, Egypt, p. 1.

Southam, G., Donald, R., Röstad, A., Brock, C., 2001. Pyrite discs in coal: evidence for fossilized bacterial colonies. Geology 29 (1), 47–50. https://doi.org/10.1130/0091-7613(2001)029<0047:PDICEF>2.0.CO;2.

Stacey, J.S., Kramers, J.D., 1975. Approximation of terrestrial lead isotope evolution by a two-stage model. Earth Planet. Sci. Lett. 26, 207–221. https://doi.org/10.1016/0012-821X(75)90088-6.

Tarhan, L.G., Droser, M.L., Gehling, J.G., Dzaugis, M.P., 2015. Taphonomy and morphology of the Ediacara form genus *Aspidella*. Precambrian Res. 257, 124–136. https://doi.org/10.1016/j.precamres.2014.11.026.

Teixeira, A.L., Gaucher, C., Paim, P.S.G., Fonseca, M.M., Filho, W.F.S., 2004. Bacias do estágio de Transição da Plataforma Sul-Americana. In: Mantesso-Neto, V., Bartorelli, A., Carneiro, C., Dal, R., Brito Neves, B.B. (Eds.), Geologia do Continente Sul-Americano: Evolução da Obra de Fernando Flávio de Almeida. Beca Produções Culturais Ltda, São Paulo, pp. 487–536.

Van Achterbergh, E., Ryan, C.G., Jackson, S.E., Griffin, W.L., 2001. Data reduction software for LA-ICP-MS: appendix. In: Sylvester, P.J. (Ed.), Laser Ablation-ICP-Mass Spectrometry in the Earth Sciences: Principles and Applications. Mineralogical Association of Canada Short Course Series 29 (Ottawa).

Walter, M.R., Bauld, J., Brock, T.D., 1972. Siliceous algal and bacterial stromatolites in hot springs and geyser effluents of Yellowstone National Park. Science 178, 402–405. https://doi.org/10.1126/science.178.4059.402.

Walter, M.R., Bauld, J., Brock, T.D., 1976. Microbiology and morphogenesis of columnar stromatolites (Conophyton, Vacerrila) from hot springs in Yellowstone National Park. In: Walter, M.R. (Ed.), Stromatolites. Elsevier, New York.

Zucatti da Rosa, A.L., 2005. Evidências de vida no Ediacarano Inferior da Bacia do Itajaí, SC. (Master dissertation). Universidade do Vale do Rio dos Sinos, São Leopoldo.